https://doi.org/10.5194/egusphere-2026-6730
Preprint. Discussion started: 5 November 2026
© Author(s) 2026. CC BY 4.0 License.

Simulating locked pastures in snow from Arctic rain events

Érika Boisvert-Vigneault[1,2,3], Melody Sandells[1], Vincent Vionnet[4], Nicolas R. Leroux[4], Nick Rutter[1], Alexandre Langlois[3,5], Hannah Bloomfield[2], and Josée-Anne Langlois[3,5]

[1]School of Geography and Natural Sciences, University of Northumbria at Newcastle, Newcastle-upon-Tyne, NE1 8ST, United Kingdom
[2]Department of Civil and Geospatial Engineering, School of Engineering, Newcastle University, Newcastle-upon-Tyne, NE1 7RU, United Kingdom
[3]Centre d'études nordiques, Université Laval, Québec, G1V 0A6, Canada
[4]Numerical Modelling and Prediction Research Division, Environment and Climate Change Canada, Dorval, H9P 1J3, Canada
[5]Département de géomatique appliquée et télédétection, Université de Sherbrooke, Sherbrooke, J1N 3C6, Canada

Correspondence: Érika Boisvert-Vigneault (erika.boisvert-vigneault@northumbria.ac.uk)

Abstract. Rain-on-snow (ROS) events occurring in the Arctic can form dense ice layers, preventing ungulates such as muskoxen and caribou from foraging throughout the winter. Such snow conditions are known as locked pastures as the vegetation is trapped beneath the dense ice layer. These locked pastures can have severe consequences for Arctic wildlife populations and Indigenous communities that depend on them. This study (1) assessed how well two meteorological reanalyses, ERA5 and the Canadian Surface Reanalysis (CaSR) v3.2, represent the meteorological conditions driving ROS events, and (2) evaluated whether the multi-physics snowpack model Crocus can reproduce the resulting locked-pasture stratigraphy. The reanalyses were evaluated against three local weather stations on Banks Island in the Canadian Arctic, for near-surface air temperature, wind speed, relative humidity, and precipitation. Four methods to determine the precipitation phase were also compared against weather observations. CaSRv3.2 paired with an atmospheric-profile-based partitioning method reproduced the timing and phase of a ROS event in 2003 most accurately and was used to drive SVS2-Crocus in an ensemble composed of four water holding capacity equations, three snow-compaction schemes, three falling snow density representations, and three wind packing variations. The ensemble reproduced a locked pasture consistent with reported snow conditions in 80 of 108 members of the ensemble for the 2003–2004 winter. Sensitivity experiments that removed either the rainfall or the accompanying warm temperatures showed that above-freezing temperatures driving melt-freeze events were the dominant driver of snowpack densification, although rainfall increased the probability of a locked pasture. A 35-year (1985–2020) simulation validated against remote sensing ROS detections identified accurately four other winters that were subject to a ROS event in late fall that resulted in a dense basal snow layer. These results show that physically based snowpack models can capture and help explain the formation of ROS-driven locked pastures once meteorological reanalysis biases are identified.

https://doi.org/10.5194/egusphere-2026-6730
Preprint. Discussion started: 5 November 2026
© Author(s) 2026. CC BY 4.0 License.

1 Introduction

In the Arctic, rain-on-snow (ROS) events are becoming more frequent as a consequence of changing meteorological conditions and have been linked to atmospheric rivers (Voveris, 2022; Lauer et al., 2023) and negative anomalies in sea-ice extent (Forbes et al., 2016; Langlois et al., 2026). As the climate is warming, sea ice extent is decreasing, contributing to the enhancement of Arctic amplification through longer ice-free sea conditions. Open water, as opposed to sea-ice, has a much lower surface albedo that increases heat absorption and, as a consequence, increases water fluxes to the atmosphere, resulting in larger precipitation events between September and November in the Canadian Arctic (Boisvert et al., 2023; Cast et al., 2026; Serreze et al., 2022). The increase in autumn rainfall events overlap with early snow onset in the same region (Mudryk et al., 2020), leading to ROS events. The latest projections from the Coupled Model Intercomparison Project 6 (CMIP6) predict increases in precipitation with an earlier transition to a rainfall-dominated Arctic in both summer and autumn (McCrystall et al., 2021). Consequently, ROS occurences in autumn will likely continue to increase in frequency and intensity across the Arctic (Dolant et al., 2018; Langlois et al., 2017, 2026; Overland, 2021; Sasseville et al., 2024).

Rainfall that happen soon after the first snowfall in the autumn-winter transition can rapidly re-freeze transforming snow surrounding the vegetation into an ice crust, hindering foraging abilities of ungulates for the rest of the winter (Johnson et al., 2016; Miller and Gunn, 2003). Such ice crusts create a "locked pasture" scenario, which can lead to famine and death of ungulates if the locked pasture area sufficiently overlaps the extent of their territory (Riseth et al., 2011; Larter and Nagy, 1994). In the context of this study, a locked pasture is defined by a basal layer of 20 mm of snow (Stien et al., 2010; Hansen et al., 2011) with a density above 350 kg m^{-3}, which is known to be sufficient to prevent foraging activities (Ouellet et al., 2017; Vikhamar-Schuler et al., 2013). Furthermore, water freezing at the soil surface releases latent heat and contributes to increase the temperature of the soil (Rennert et al., 2009; Woo and Heron, 1981), promoting the growth of fungi and mold in the vegetation that affect the health of foraging animals (Kumpula et al., 2000).

In the Canadian Arctic, both muskoxen (*Ovibos moschatus*) and Peary caribou (*Rangifer tarandus pearyi*) have had severe population declines due to ROS events (i.e. Grenfell and Putkonen, 2008; Johnson et al., 2016; Larter and Nagy, 1994; Nagy et al., 1996). Peary caribou, an endemic species of northern Canada, was officially listed as "*endangered*" in 2011 as a consequence of severe icing episodes that reduced the population to 28% of its original size (Governement of Canada, 2002). Its status was revised in 2015 updating the designation to "*threatened*", due to a population increase but also considering current and future environmental pressures such as ROS events and decreased sea ice extent and thickness (COSEWIC, 2015). Both caribou and muskoxen are important species for Inuit communities, providing essential food and raw materials that are at the heart of Inuit diet, economy, and traditional practices (Taylor, 2005; Tomaselli et al., 2018). A better understanding of the formation of locked pastures could support wildlife management decisions and, in turn, help mitigate the consequences of ROS events for ungulate populations and the Inuit communities that rely on them for food, economy and traditional practices.

Investigating the spatial and temporal distribution of locked pastures cannot be done through direct remote sensing measurements: this is why wet snow detections are often used as a proxy (Vickers et al., 2022; Dolant et al., 2016; Bartsch et al., 2010). While this method provides a good estimation for ROS occurrences, with some methods obtaining up to 86 % accuracy (Pan

https://doi.org/10.5194/egusphere-2026-6730
Preprint. Discussion started: 5 November 2026
© Author(s) 2026. CC BY 4.0 License.

et al., 2018), it does not represent occurrences of locked pastures, as not all ROS event lead to severe icing conditions that are sufficient to hinder foraging (Bartsch et al., 2010; Larter and Nagy, 1994; Komarov and Stroeve, 2026). Another approach to identifying past locked pastures uses snow models to simulate snow conditions. Vikhamar-Schuler et al. (2013); Ouellet et al. (2017) and Martineau et al. (2022) have shown correlations between the cumulative thickness of snow layers exceeding a density of 350 kg m^{-3} of a full winter season and ungulate counts and grazing areas. Snow simulations allow to capture different processes that can lead to high snow density, such as wind packing, melt-refreeze or ROS events. The usage of snow models to investigate specifically the impacts of ROS events on the snowpack is restricted to studies focusing on the resulting snowmelt and water run-off (i.e. Bonsoms et al., 2024; Marsh and Pomeroy, 1996; Würzer et al., 2016). To the authors knowledge, no study have yet focused on simulating locked pastures in the Arctic from autumn ROS events. A snow model ability to simulate in-situ snow conditions is limited to the performance of Arctic snow physical properties representation and to the accuracy of the driving meteorological data.

The main limitations in Arctic physical processes within snow models include the absence water-vapour fluxes schemes (Domine et al., 2019; Menard et al., 2024) and limited wind-induced compaction (Royer et al., 2021b; Barrere et al., 2017). Both constraints limit considerably the ability of snow models to simulate Arctic tundra snow density profiles where the snowpack is composed of three main layers : a hard wind slab (at the surface), faceted crystals (intermediate) and low density large depth hoar (on the ground) (Royer et al., 2021a). As a result, some multi-layer snowpack models have been parameterized for Arctic snow, such as Crocus within the Soil, Vegetation and Snow version 2 (SVS2) land surface model (Vionnet et al., 2012, 2025; Woolley et al., 2024), SNOWPACK (Bartelt and Lehning, 2002; Martineau et al., 2022) and SnowModel (Liston and Elder, 2006; Pflug et al., 2019). While these parametrizations better simulate Arctic snowpacks, the use of a multiphysics approach would allow to quantify uncertainties associated with the snowpack model and the impact on the simulation of locked pasture.

In the case of meteorological data limitations, one of the main challenges when investigating ROS events is to identify the phase of precipitation around the time of the event, where misidentifying the precipitation phase can be the difference between a ROS event, snowfall or a rain-on-ground event. Precipitation partitioning methods (PPMs) are used to distinguish between solid and liquid precipitations and rely on meteorological variables such as near-surface air temperature, humidity and atmospheric pressure (i.e. Harder and Pomeroy, 2013; Jennings et al., 2018; Leroux et al., 2023; Wang et al., 2019). To identify the precipitation phase, a temperature threshold can be used, based on either a theoretical value (Loeb et al., 2022) or one calculated from in-situ measurements, where thresholds for rain can range from 0.8°C to 2.4°C (Jennings et al., 2018; Madore et al., 2023). More complex method that integrate other meteorological variable can allow for more than only solid and liquid precipitation. Harder and Pomeroy (2013) and Wang et al. (2019) both suggested equations to calculate the liquid precipitation fraction based on near-surface air temperature and 2-m relative humidity, allowing for mixed precipitation that are expected to be more realistic when temperatures are oscillating around 0°C. In the case of Bourgouin (2000), the vertical air temperature profile is used to identify four precipitation types: snow, rain, freezing rain and ice pellets.

Meteorological variables required to calculate different PPMs and to drive snowpack models are, for the most part, available in standard weather station dataset. However, weather stations are scarce in the Arctic and are associated with limited quality

https://doi.org/10.5194/egusphere-2026-6730
Preprint. Discussion started: 5 November 2026
© Author(s) 2026. CC BY 4.0 License.

due to the harsh environment. As a consequence, meteorological reanalyses offer a potential to drive distributed snowpack simulations to inform about the state of the snowpack across large areas and in particular the formation of locked pasture. Atmospheric reanalyses assimilate historical observations into a fixed numerical weather prediction model to produce consistent, gridded records of the atmospheric state. Yet, their reliability is limited in the Arctic by a sparse and spatially biased observing network, which leaves large areas of ocean and land weakly constrained by assimilated data (Laroche and Poan, 2022; Lawrence et al., 2019). This limitation is compounded by the difficulty models have in representing stable boundary layers, mixed-phase clouds, and snow-atmosphere interactions, leading to persistent biases in near-surface temperature, precipitation, and snowfall. Evaluating the accuracy of the driving reanalysis data is therefore a necessary step when modelling Arctic snowpacks, as biases in temperature and precipitation phase can determine whether ROS events are correctly detected and, in turn, whether locked pasture conditions are reliably identified.

To investigate ROS events in the Arctic and how they are represented within snowpack models, this study focuses on Banks Island, located in the Canadian Arctic Archipelago, which has been the subject of multiple ROS events that led to rapid declines in caribou and muskoxen populations in the past (Langlois et al., 2026; Larter and Nagy, 1994; Nagy et al., 1996). A major ROS events occurred in early October 2003 on Banks Island, which formed an ice layer too thick for muskoxen to penetrate and access vegetation for foraging, leading to the loss of about 25 % of the muskoxen population of the island (Grenfell and Putkonen, 2008; Putkonen et al., 2009). The October 2003 ROS event is the best documented one, with reports of weather and snow cover conditions available to validate both meteorological reanalyses and the snowpack model. A multi-year simulation was also completed to investigate the simulation of locked pastures through different meteorological conditions. This study aims to:

- Assess whether meteorological reanalyses can capture key elements of ROS events that lead to locked pastures.
- Evaluate the capacity of a physical snowpack model (SVS2-Crocus) to recreate locked pasture stratigraphy in Arctic snow conditions as a result of ROS events.

Section 2 describes the study site, the configuration of the SVS2-Crocus ensemble, followed by an overview of the meteorological reanalyses used, measurements, observations and calculations of precipitation phase and finally the explanation of the experimental setup. Results are presented in Section 3, where the accuracy of meteorological reanalyses and PPMs are evaluated and the ability of SVS2-Crocus to reproduce locked pastures for the 2003 ROS event and a 35 years time-series is assessed. Section 4 discusses the implications of these results and conclusions are presented in Section 5.

https://doi.org/10.5194/egusphere-2026-6730
Preprint. Discussion started: 5 November 2026
© Author(s) 2026. CC BY 4.0 License.

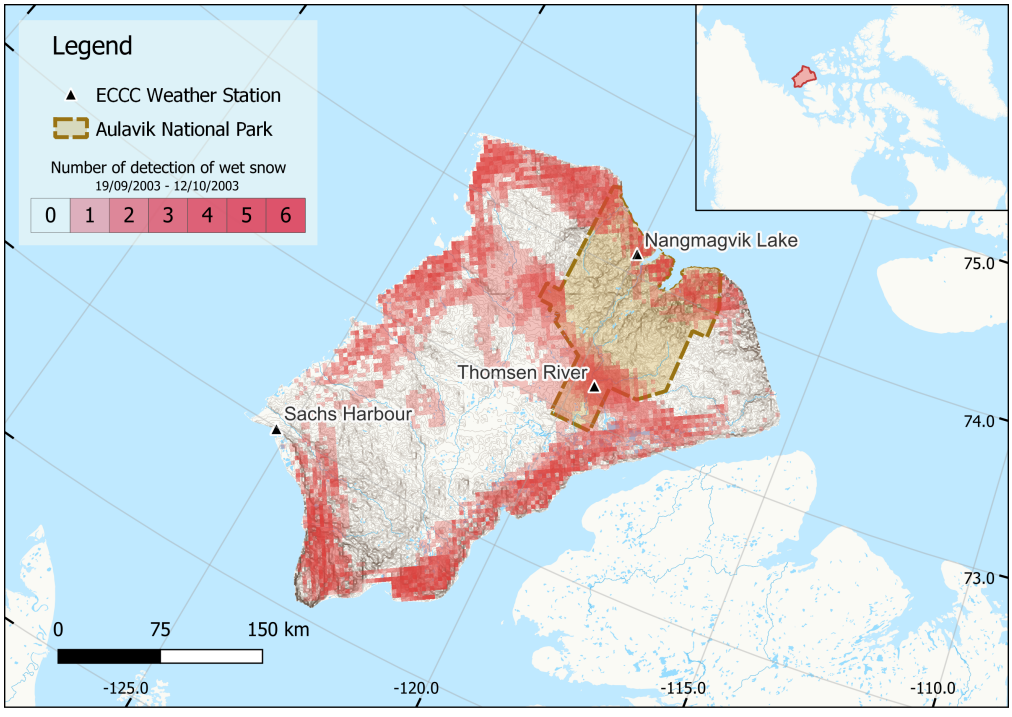


Figure 1. Map of Banks Island showing the location of positive detections of ROS from Langlois et al. (2026) and the location of three local weather stations from Environment and Climate Change Canada.

2 Data and methods

2.1 Study area

2.1.1 Banks Island

Banks Island is part of the Inuvialuit Settlement Region, located in the southwest of the Canadian Arctic Archipelago, and covers an area of about 70,000 km^2. The island is a lowland terrain consisting of a tundra ecosystem composed mainly of dwarf shrubs, grasses, sedges, and flowering plants that is settled in a thin active layer of soil (between 50 and 75 cm) above continuous permafrost (French, 2017). Sachs Harbour (Ikaahuk) is the only settlement on Banks Island, situated in the southwest of the isle (Figure 1). It is also home to two ungulate species that are essential to traditional activities of Inuit communities: the Peary caribou and muskoxen (Johnson et al., 2016; Davison et al., 2017; Parks Canada Agency, 2025). In the northeast, the Aulavik National Park protects about 17 % of the island surface area (Parks Canada Agency, 2025). As shown in Figure 1, the national park encompasses two out of the three weather station of Environment and Climate Change Canada (ECCC): Thomsen River (lon: 119.54°W; lat: 73.23°N, alt: 28 m) and Nangmagvik Lake (lon: 119.99°W; lat: 74.14°N; alt: 19 m). The third local weather station (LWS) is located within the community of Sachs Harbour (lon: 125.27°W; lat: 72.00°N; alt: 54 m).

https://doi.org/10.5194/egusphere-2026-6730
Preprint. Discussion started: 5 November 2026
© Author(s) 2026. CC BY 4.0 License.

2.1.2 Local weather station (LWS) data

Meteorological reanalyses were evaluated against data from ECCC weather stations at three locations on Banks Island (see Figure 1 for locations). The three ECCC weather stations are the only ones located on Banks Island whose data is publicly available. 2-m relative humidity, 2-m air temperature, 10-m wind speed and direction, and surface air pressure are available at an hourly resolution at Nangmagvik Lake since 1996, Thomsen River since 1997, and Sachs Harbour since 1955.

Sachs Harbour weather station is staffed, resulting in data being only available between 09:00 and 17:00 with two additional entries at 05:00 and 23:00 LT, including weather conditions. Observed weather conditions provide hourly indications of precipitation type (i.e. rain, drizzle, ice pellets, freezing rain, etc.), precipitation intensity (i.e. heavy drizzle, moderate snow showers, etc.), and general weather conditions (i.e. mostly clear, thunderstorm, fog, cloudy, etc.). Reported precipitation type at Sachs Harbour was used to validate the different precipitation phase partitioning methods (PPMs) (Section 2.4.1), where mentions of drizzle or rain (including freezing rain) were qualified as liquid precipitation and snow, ice pellets or hail were considered solid precipitation. Within the entire database of weather conditions between 1980 and 2020, observations of mixed precipitation occur in only 0.13 % of cases (146 out of 109 492 precipitation observations). Due to the rarity of mixed precipitation events, they have been excluded from the dataset.

Sachs Harbour is also the only station on Banks Island where information about the precipitation gauge type is readily available, allowing for precipitation data records to be corrected accordingly for wind-induced undercatch. Daily precipitation amounts at Sachs Harbour were corrected for the period between 1955 and 2013 by Wang et al. (2017) in the Adjusted Daily Rainfall and Snowfall Dataset for Canada. Corrected daily precipitation amounts were compared to total daily precipitation from meteorological reanalyses. For the analysis, a minimum threshold of 0.2 mm for total daily precipitation was applied to meteorological reanalyses to define a day with precipitation, based on the smallest amount of precipitation (trace) that weather station gauges can measure (Environment and Climate Change Canada).

2.2 Snowpack model SVS2-Crocus Configuration

Crocus is a multilayer snowpack model (Brun et al., 1992; Vionnet et al., 2012; Lafaysse et al., 2026) and was integrated within the SVS2 land surface model (Vionnet et al., 2025). Soil texture and vegetation characteristics were extracted from the SoilGrids 2.0 database (Poggio et al., 2021) and French (2017). Since the Thomsen River is not located in an area that is covered by shrubs, the height of Arctic vegetation has been set to 0 cm. As a consequence, the effect of Arctic vegetation on basal snowpack properties (Royer et al., 2021b; Woolley et al., 2024) are not simulated. A complete list of options and physical parameters used in this study can be found in Appendix B. To investigate the ability of SVS2-Crocus to recreate a locked pasture, different schemes driving liquid water percolation and snow density were tested through an ensemble approach. Each physical representation used in the ensemble is described in Table 1 and in the following paragraph.

In SVS2-Crocus, the water percolation scheme is a *bucket approach*, meaning that an input of liquid water in the snowpack from either rainfall or snowmelt first fills the surface snow layer until it reaches its maximum water holding capacity. Excess water then flows into the layer underneath. SVS2-Crocus has four physical processes describing maximum water holding

https://doi.org/10.5194/egusphere-2026-6730
Preprint. Discussion started: 5 November 2026
© Author(s) 2026. CC BY 4.0 License.

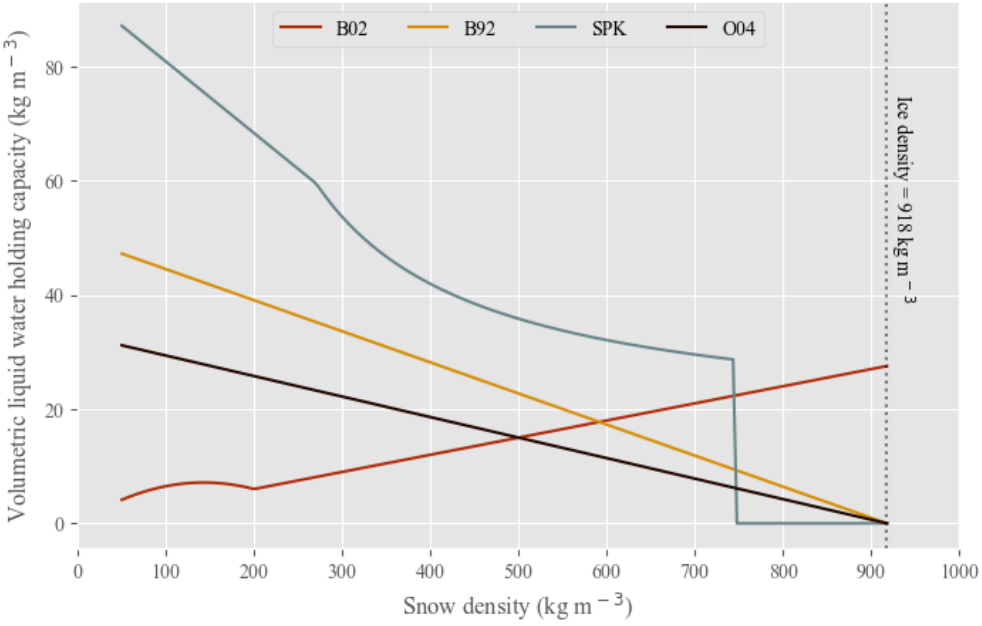


Figure 2. Behaviour of different parameters of water holding capacity implemented in SVS2-Crocus as a function of snow density.

capacity representations implemented, defined in Table 1: B02, B92, SPK and O04. All equations depend on snow layer density, as shown in Figure 2, where SPK, B92 and O04 are associated with a negative relationship between snow density and volumetric water holding capacity, whereas B02 exhibits a positive relationship. SPK has a threshold at 747 kg m^{-3} where the snow layer becomes impermeable. In the specific case of liquid precipitation at temperatures below 0°C, a modification of the B92 percolation scheme for freezing rain is triggered, causing a rapid increase in the water holding capacity of the first 2 cm at the surface to simulate ice impermeability (Quéno et al., 2018). This function allows the formation of an ice layer at the surface of the snowpack, simulating the consequences of a freezing rain event.

The main physical processes affecting directly snow density in SVS2-Crocus are the snow compaction, wind packing and falling snow density schemes. Three snow compaction schemes were tested in this study: B92, T11 and S14 . In the case of wind-packing and falling snow density, Arctic parameterizations implemented through the work of Woolley et al. (2024) have been used in this study (Table 1). Three representations of wind packing, R21W, R21R and R21F, increase both the rate and the maximum density attainable through wind packing when compared to other default options available in SVS2-Crocus, and three falling snow density equations increase the impact of wind speed by a factor of 2, 1.5 and 1.25 respectively for R21, GW1 and GW2.

https://doi.org/10.5194/egusphere-2026-6730
Preprint. Discussion started: 5 November 2026
© Author(s) 2026. CC BY 4.0 License.

Table 1. Description of SVS2-Crocus model ensemble equations.

Source	Reference name	Description
		Water holding capacity
Brun et al. (1992)	B92	Volumetric liquid water holding capacity corresponds to 5% of pore volume (Eq. 9, Lafaysse et al., 2017)
Boone (2002)	B02	Water retention capacity defined by a maximal liquid water mass fraction (Eq. 13, Lafaysse et al., 2017).
Oleson et al. (2004)	O04	Volumetric liquid water holding capacity corresponds to 3.3% of pore volume (Eq. 7.26, Oleson et al., 2004).
Wever et al. (2014)	SPK	Water holding capacity as a function of snow porosity depending on the volumetric ice content of the layer (Eq. 12, Lafaysse et al., 2017).
		Snow compaction
Brun et al. (1992)	B92	Viscosity defined as a function of snow density and temperature (Eq. 15, Lafaysse et al., 2017).
Teufelsbauer (2011)	T11	Viscosity defined as a function of snow density and temperature (Eq. 16, Lafaysse et al., 2017).
Schleef et al. (2014)	S14	Defined as the compaction rate integrating snow microstructure (specific surface area) within the first h after snowfall (Eq. 17, Lafaysse et al., 2017).
		wind packing
Royer et al. (2021b)	R21W	Triples the wind effect coefficient to account for underestimating the effect of wind on surface snow density (Eq. 3, Woolley et al., 2024)
Barrere et al. (2017); Lackner et al. (2022); Royer et al. (2021b)	R21R	Increases the maximum density of snow impacted by wind from 350 to 600 kg m^{-3} (Eq. 2, Woolley et al., 2024)
Woolley et al. (2024)	R21F	Combination of both R21W and R21R (Eqs. 2 and 3, Woolley et al., 2024)
		Falling snow density
Royer et al. (2021b)	R21	Doubles the wind speed factor in the calculation of falling snow density from 26 to 52 kg $m^{-7/2}s^{1/2}$ (Eq. 1, Woolley et al., 2024)
Woolley et al. (2024)	GW1	Increases the wind speed factor in the calculation of falling snow density from 26 to 39 kg $m^{-7/2}s^{1/2}$ (Eq. 1, Woolley et al., 2024)
Woolley et al. (2024)	GW2	Increases the wind speed factor in the calculation of falling snow density from 26 to 32.5 kg $m^{-7/2}s^{1/2}$ (Eq. 1, Woolley et al., 2024)

https://doi.org/10.5194/egusphere-2026-6730
Preprint. Discussion started: 5 November 2026
© Author(s) 2026. CC BY 4.0 License.

2.3 Meteorological reanalyses

ERA5 and CaSRv3.2 are meteorological reanalyses that cover the Canadian Arctic, with large temporal ranges, respectively from 1940 to present and 1980 to 2025, at hourly temporal resolution, allowing for long-term comparison with LWS. ERA5 is produced by the European Centre for Medium-range Weather Forecasts (ECMWF) and has a spatial resolution of 0.25°(Hersbach et al., 2020). Graham et al. (2019) showed that ERA5 performs better than other atmospheric reanalyses across the Arctic, exhibiting better correlations with observations for temperature, wind speed, and humidity. In the context of this study, ERA5 data were extracted at the location of three LWS on Banks Island (see Figure 1) from 1980 onwards to match the temporal range of the CaSRv3.2 dataset. ERA5 data were interpolated to the station location using bilinear interpolation for hourly 2 m air temperature and specific humidity, 10 m wind speed, longwave and shortwave radiation, and nearest neighbour interpolation for precipitation.

CaSRv3.2 is a 10-km North American precipitation and land surface reanalysis created from the global deterministic reforecast system (GDRS) initialized with ERA5 from 1980. Outputs from GDRS were dynamically downscaled from 0.25°to $\sim$10 km using the regional deterministic reforecast system coupled with the Canadian Land Data Assimilation System (CaLDAS) and precipitation analysis (CaPA) to produce the final CaSRv3.2 product (Khedhaouiria et al., 2026). Compared to previous versions, CaSRv3.2 has been shown to have a reduced bias in data-sparse regions, like the Canadian Arctic, especially through its representation of precipitation events (Khedhaouiria et al., 2026), which is key when investigating ROS events. Two precipitation outputs are available for CaSRv3.2: (i) the raw precipitation forecast of the model, hereafter referred to as CaSRv3.2-F, and (ii) the analysed precipitation of CaPA that blends surface station observations and the raw precipitation forecast, hereafter referred to as CaSRv3.2-R. It is important to note that the dataset from which the surface station observations are extracted is the Adjusted Daily Rainfall and Snowfall Dataset for Canada (Wang et al., 2017), which includes the precipitation data from Sachs Harbour (Khedhaouiria et al., 2026). Therefore, comparison of CaSRv3.2-R precipitation amounts and timing with Sachs Harbour is not independent. However, both precipitation outputs are considered in this study due to the scarcity and limited reliability of in-situ precipitation data in the Arctic (Laroche and Poan, 2022; Lawrence et al., 2019). CaSRv3.2 data were extracted at the location of all three LWS on Banks Island (see Figure 1) from 1980 onwards.

Relative humidity with respect to liquid water over the full range of temperature, 2-m air temperature and 10 m wind speed from meteorological reanalyses were compared against LWS measurements due to their relevance in determining precipitation phase (see Section 2.4.1) and in driving the forcing for snowpack simulations (see Section 2.2). Biases and root mean square differences (RMSD) were calculated at all three LWS for each reanalysis over the complete dataset and for near-freezing periods, when the temperature recorded at the LWS ranged between -5 and 5°C. For wind speed and relative humidity during near-freezing periods, a maximum difference of 5°C was tolerated between the observed and the reanalysis surface air temperatures. The focus on near-freezing periods aims to refine the dataset to only periods where ROS events could potentially happen.

The Frequency Bias Index (FBI), Equitable Threat Score (ETS) and proportion of correctly detected events (PC) were calculated from a 2×2 contingency table of presence/absence of daily precipitation for each meteorological reanalysis at Sachs

https://doi.org/10.5194/egusphere-2026-6730
Preprint. Discussion started: 5 November 2026
© Author(s) 2026. CC BY 4.0 License.

Harbour. FBI is the ratio of predicted events over total observed occurrences, while ETS quantifies true predicted events after accounting for occurrences expected by random chance. Further details about the calculation of the FBI, ETS and PC can be found in Appendix A.

2.4 Precipitation Phase

2.4.1 Phase Partitioning Methods (PPMs)

Meteorological data used as an input to snowpack models like SVS2-Crocus require the specification of the phase of precipitation (solid or liquid). Different PPMs were used to derive the liquid and solid precipitation rates from the total precipitation available in the different reanalyses. A total of four different PPMs (Table 2) were tested: (a) three ground-based PPMs, which only rely on near-surface temperature and humidity, and (b) one atmospheric-based PPM, which accounts for the vertical profile of upper-air temperature and is specific to CaSR3.2. PPMs were evaluated against Sachs Harbour precipitation phase observations to determine their suitability to identify ROS events.

The first method used a spatially variable near-surface air temperature threshold extracted from the work of Jennings et al. (2018), hereafter referred to as "J18". Air temperature threshold for Sachs Harbour was 1.22°C , where precipitation above the threshold was considered liquid and below was considered solid. More complex methods such as those using the wet-bulb temperature (W19, Wang et al., 2019), which corresponds to the lowest temperature attainable through evaporative cooling, and the hydrometeor temperature method (HP13, Harder and Pomeroy, 2013), were also analysed. Both W19 and HP13 generate a liquid fraction between 0 and 1. For the purpose of this study, because mixed precipitation was removed from the analysis, liquid fractions greater than 0.5 were considered liquid and those below 0.5, solid. All three ground-based PPMs, J18, W19 and HP13, were applied to the two reanalysis products. The remaining atmospheric-based PPM is based on Bourgouin (2000) (B00) and used vertical profiles of air temperature to identify four different precipitation types: rain, freezing rain, snow and ice pellets. A summary of PPM methodology can be found in Table 2. By default, the outputs of B00 are only available for CaSRv3.2-F at an hourly time scale. In the context of this study, they have reprocessed to provide a phase separation that matches the total precipitation amount of CaSRv3.2-R. The comparison with precipitation phase observations focused on near-freezing periods where air temperatures recorded at Sachs Harbour were between -5°C and 5°C and the modelled air temperature was within 5°C of the LWS measurement. Skill scores (FBI, ETS and PC, defined in Section 2.3) were calculated for each precipitation phase when both observations and the compared model-PPM pairing agreed on the presence of precipitation. The percentage of correctly detected events was also calculated to help identify which model-PPM pairing was the most appropriate.

In addition, the ability of each PPM to reproduce liquid precipitation for the ROS event of October 2003 at Thomsen River was assessed by comparing the timing of liquid precipitation and the near-surface air temperature to positive ROS detections from Langlois et al. (2026) (Section 2.4.2). The combination of meteorological reanalysis and PPM that showed the best fit with precipitation phase and timing was subsequently used as meteorological forcing for SVS2-Crocus.

https://doi.org/10.5194/egusphere-2026-6730
Preprint. Discussion started: 5 November 2026
© Author(s) 2026. CC BY 4.0 License.

Table 2. Description of precipitation phase partitioning methods.

Source (reference name)	Description	Output	Meteorological reanalysis
Jennings et al. (2018) (J18)	Spatially distributed near-surface rain-snow temperature threshold. *Sachs Harbour: 1.22°C*	Rain (liquid); Snow (solid)	CaSRv3.2; ERA5
Wang et al. (2019) (W19)	Index (f_r) calculated from the near-surface wet-bulb temperature (T_W): $f_r = 1 - \frac{1}{1+ae^{b(T_w+c)}}$ $a = 6.99 \times 10^{-5}$ $b = 2.0\ \mathrm{K}^{-1}$ $c = 3.97\ \mathrm{K}$	Liquid precipitation fraction (0–1)	CaSRv3.2; ERA5
Harder and Pomeroy (2013) (HP13)	Index calculated from hydrometeor temperature (T_i): $f_r = \frac{1}{1+\alpha\beta^{T_i}}$ $\alpha = 2.50286$ $\beta = 0.125006$	Liquid precipitation fraction (0–1)	CaSRv3.2; ERA5
Bourgouin (2000) (B00)	Distinction of precipitation phase based on vertical temperature profile and the thickness of atmospheric layers.	Rain (liquid); Freezing rain (liquid); Snow (solid); Ice pellets (solid)	CaSRv3.2

2.4.2 Remote sensing detection

Langlois et al. (2026) developed a high resolution (3.125 km) dataset of ROS detection for Banks Island from 1987 to 2023 based on passive microwave satellite measurements at 19 and 37 GHz. The passive microwave algorithm triggers a positive detection when enough water is present near the surface of the snowpack (Dolant et al., 2017). The minimum amount of water at the surface of the snowpack required to obtain a positive wet snow detection varies based on the threshold of the polarized gradient ratio (GRP) used in the analysis, although no direct quantity of water is associated with GRPs. In the case of Langlois et al. (2026), the GRP used was -2, which is more sensitive to wet snow than previous works from Dolant et al. (2017) and Sasseville et al. (2024), both using a GRP of -10. To increase the accuracy of the remote sensing dataset, Langlois et al. (2026) validated the results of the wet snow detections with the presence of snow cover using National Oceanic and Atmospheric Administration (NOAA) snow cover maps (Robinson et al., 2012). Finally, a cluster analysis was done in Langlois et al. (2026) to identify only major events that would have had negative impacts on the local fauna.

The remote sensing ROS detection dataset of Langlois et al. (2026) was used in this study to validate when and where ROS events happened on Banks Island, indicating potential locked pastures within the snowpack. To evaluate whether the snowpack

https://doi.org/10.5194/egusphere-2026-6730
Preprint. Discussion started: 5 November 2026
© Author(s) 2026. CC BY 4.0 License.

model was able to recreate a locked pasture from a ROS event, the major ROS event of October 2003, which caused the death of more than 20 000 muskoxen, was used as a case study due to the availability of in-situ observations. A large number of positive detections of ROS were measured on Banks Island between 19 September 2003 and 12 October 2003 (Langlois et al., 2026). Positive detections of ROS happened at Thomsen River in four instances of satellite passages (one in the morning and one in the evening) between 2 and 5 October 2003, shown in red in Figure 1. Then, the number of positive ROS detections was counted for each winter from 1987 to 2020, at the location of the Thomsen River again and compared to a long-term simulation of the snowpack at this location. For the historical count of ROS detections at Thomsen River, a GRP of -2 was used and the snow cover was validated with the NOAA snow cover maps, but no cluster analysis was carried out, allowing all positive detections for this specific location to be retained for comparison with the snowpack model.

2.4.3 In-situ observations

Community members of Sachs Harbour provided evidence of the snow conditions during and after the ROS event of 2003 on Banks Island. According to Rennert et al. (2009), hunters reported that about 15 cm of new snow had accumulated on the island before "a week of intermittent [drizzly] rains and a rapid return to subfreezing temperatures" formed a "thick sheet of ground-fast ice on the northern two-thirds of the island". The described conditions indicate that the amount of precipitation was low since the ROS event corresponded to intermittent drizzly rain. From the depiction of the events, it is possible to interpret that the $\sim$15 cm of fresh snow filled with liquid water throughout the week of drizzly rain, after which it re-froze completely, creating a thick and potentially dense layer of melt forms on the soil surface. The resulting icy basal snow layer is considered to be a locked pasture.

2.5 Experimental setup

Altogether, the four water holding capacity equations, three snow compaction schemes, three wind packing representations, and three falling snow density variations available in SVS2-Crocus form a 108-member ensemble. Ensemble simulations were run at Thomsen River from July 1998 to June 2004, forced by the meteorological reanalysis with the lowest error in capturing the ROS event. A 5-year spin-up was run by using the forcing between 1998-2003 to correctly initialize the soil conditions at the beginning of the simulation period. Analysis of the modelled density and stratigraphy of the snowpack for the 2003–2004 winter was completed to provide an estimate of the model's capacity to recreate locked pastures, through comparison with conditions reported by hunters from Sachs Harbour in Rennert et al. (2009) (Section 2.4.3. Simulation of a locked pasture is identified where a 20 mm layer at the base of the snowpack exceeds 350 kg m^{-3} (Vikhamar-Schuler et al., 2013; Ouellet et al., 2017).

An additional two simulations using the 108-member ensemble approach for the same period were completed to better understand the processes that lead to the formation of a locked pasture. Changes in the meteorological driving data were made between 19 September 2003 and 12 October 2003, which represents the entire length of the ROS event of 2003 on Banks Island. In the first scenario, hereafter referred to as the cold simulation, maximum surface air temperatures were set to -0.5°C between 19 September 2003 and 12 October 2003 to limit snowmelt from interfering with the formation of the locked pasture.

https://doi.org/10.5194/egusphere-2026-6730
Preprint. Discussion started: 5 November 2026
© Author(s) 2026. CC BY 4.0 License.

The precipitation phase was maintained to promote freezing rain. In the second scenario, hereafter referred to as the no-rain simulation, all liquid precipitation was turned into snowfall between 19 September 2003 and 12 October 2003, allowing the impacts of snowmelt on the formation of a locked pasture to be isolated.

To verify that the snowpack model can simulate locked pastures in different ROS conditions, a long-term simulation was also completed from 1980 to 2020 at Thomsen River, using the same 108-members ensemble as before. Once again, the first 5 years of the simulation were used to spin up the model, producing results only for the period between 1985 and 2020. Densities above 350 kg m^{-3} were extracted for 31 October of every year, as no ROS were detected after this date by Langlois et al. (2026) and allowing a few days after the ROS event for the water to settle (Woo and Heron, 1981), capturing only locked pastures caused by early snow season melt or ROS events. Snow stratigraphy was then evaluated against historical positive ROS detections at the location of Thomsen River, extracted from the work of Langlois et al. (2026). Furthermore, to confirm potential locked pastures, five years with reported ROS events associated with ungulate die-offs on Banks Island (1987, 1988, 1990, 1993 and 2003 from Table 3 of Langlois et al., 2026) are verified against the model's snow stratigraphy.

3 Results

This section first focuses on the accuracy of meteorological reanalyses, which includes both near-surface variables and PPM performances. The meteorological reanalysis and PPM pairing that captured best the precipitation phase and timing is identified and results of the snowpack model ensemble simulations are presented, followed by the historical assessment of locked pastures.

3.1 Accuracy of meteorological reanalyses

3.1.1 Air temperature, wind speed and relative humidity

For the full dataset, ERA5 outperformed CaSRv3.2 for air temperature at all three LWS, with biases closer to 0 (from -0.11 to 0.53°C for ERA5, compared with 1.10 to 1.55°C for CaSRv3.2) and lower RMSDs (2.32 to 2.95°C and 3.29 to 3.37°C, respectively). Air temperature was the only variable with a high correlation ($R^2 > 0.8$) for both reanalyses, with values between 0.94 and 0.98 across all LWS. Near-freezing periods represented between 21 and 27 % of the full dataset, depending on the LWS and the reanalysis considered (see Appendix C for exact numbers). In these periods, RMSDs were lower than for the full dataset for both reanalyses, from an average of 3.34 to 1.67°C for CaSRv3.2 and from 2.54 to 1.22°C for ERA5, and ERA5, again, showed the lowest RMSDs at all LWS. ERA5 also had overall higher correlation coefficients than CaSRv3.2 in near-freezing periods (see Table 3). No systematic pattern was identified in air temperature bias, although positive biases (overestimation) were more frequent across the sample, mostly driven by CaSRv3.2, which overestimated air temperature at all LWS for the full dataset.

Wind speed was underestimated by both reanalyses at all LWS, over the full dataset as well as in near-freezing periods. Over the full dataset, the negative bias was smaller for ERA5 (-0.57 to -0.21 m s^{-1}) than for CaSRv3.2 (-1.10 to -0.86 m s^{-1}), and

https://doi.org/10.5194/egusphere-2026-6730
Preprint. Discussion started: 5 November 2026
© Author(s) 2026. CC BY 4.0 License.

Table 3. Bias (RMSD) for surface air temperature, wind speed and relative humidity for the two reanalysis at all three LWS on Banks Island over (i) the complete dataset and (ii) near-freezing periods only. Asterisks identify strong correlations, where one ($*$) corresponds to $R^2 > 0.5$ and two ($**$) corresponds to $R^2 > 0.8$.

Variable	Reanalysis	Sachs Harbour	Nangmagvik Lake	Thomsen River
		(i) Full dataset		
Air temperature (°C)	ERA5	0.35 (2.32)**	0.53 (2.95)**	−0.11 (2.35)**
	CaSRv3.2	1.23 (3.36)**	1.10 (3.29)**	1.55 (3.37)**
Wind speed (m s^{-1})	ERA5	−0.57 (2.10)*	−0.21 (2.03)*	−0.28 (2.16)*
	CaSRv3.2	−1.03 (2.31)*	−1.10 (2.26)*	−0.86 (2.18)*
Relative humidity (%)	ERA5	−2.80 (8.27)	−0.96 (7.45)*	−1.26 (7.37)*
	CaSRv3.2	−4.12 (9.30)	−2.93 (7.86)*	−3.73 (8.32)*
		(ii) Near-freezing periods		
2 m Air temperature (°C)	ERA5	0.65 (1.27)**	−0.27 (1.21)**	−0.53 (1.18)**
	CaSRv3.2	0.88 (1.74)*	−0.06 (1.61)*	0.62 (1.65)*
Wind speed (m s^{-1})	ERA5	−0.80 (2.00)*	−0.77 (1.83)*	−0.91 (1.86)*
	CaSRv3.2	−0.84 (2.00)*	−1.23 (2.07)*	−0.92 (1.83)*
Relative humidity (%)	ERA5	−5.40 (8.78)	−3.87 (7.83)	−5.04 (8.45)
	CaSRv3.2	−7.28 (10.50)	−5.93 (9.22)	−7.39 (10.41)

ERA5 also had the lower RMSDs (2.03 to 2.16 m s^{-1}, compared with 2.18 to 2.31 m s^{-1} for CaSRv3.2). Correlations were moderate for both products ($R^2 > 0.5$) but never exceeded 0.8 (see Table 3). In near-freezing periods, RMSDs were lower than for the full dataset (1.83 to 2.00 m s^{-1} for ERA5 and 1.83 to 2.07 m s^{-1} for CaSRv3.2). Figure 3 shows that both reanalyses followed a similar pattern at all LWS. Wind speed was slightly overestimated during periods of measured calm, more so for ERA5, and the modelled quantiles progressively fell below the 1:1 line as measured wind speed increased. This underestimation of the upper quantiles was weakest at Sachs Harbour, where the highest modelled quantiles reached 11.5 m s^{-1} for measured values of about 13.5 m s^{-1}, while at Thomsen River and Nangmagvik Lake, modelled quantiles did not exceed 10 m s^{-1} for similar measured wind speeds, indicating that stronger wind events were not captured.

In the case of relative humidity, both reanalyses display much larger biases and RMSD than for air temperature and wind speed. Both ERA5 and CaSRv3.2 produced a negative bias at all LWS and in both periods, indicating that modelled air was systematically drier than observed. Over the full dataset, ERA5 biases ranged from -2.80 to -0.96 % and RMSDs from 7.37 to 8.27 %, while CaSRv3.2 showed larger biases (-4.12 to -2.93 %) and RMSDs (7.86 to 9.30 %). Correlations were also weak: R^2 exceeded 0.5 only at Nangmagvik Lake and Thomsen River (see Table 3), and remained below this threshold at Sachs Harbour. The performance of both reanalyses decreased during near-freezing periods: biases increased considerably (from -1.67 to -4.77 % on average for ERA5 and from -3.59 to -6.87 % for CaSRv3.2) and R^2 fell below 0.5 at all LWS. Despite a poorer performance in near-freezing periods, ERA5 still has the lower bias and RMSD at all LWS in both periods.

https://doi.org/10.5194/egusphere-2026-6730
Preprint. Discussion started: 5 November 2026
© Author(s) 2026. CC BY 4.0 License.

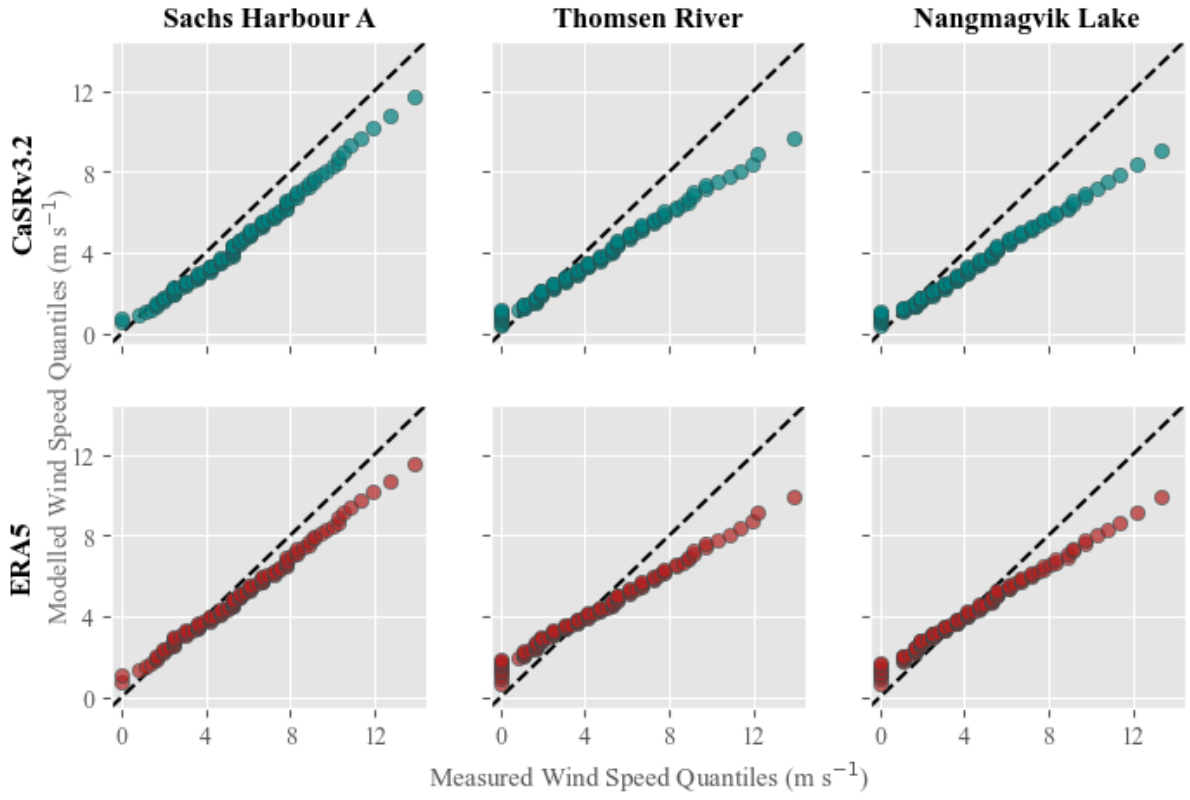


Figure 3. Quantile-quantile plots of wind speed (m s^{-1}) comparing observations to reanalyses for the full dataset. See Figure 1 for the locations of weather stations.

3.1.2 Total precipitation

The daily occurrence of precipitation in the three products considered in this study (CaSRv3.2-F, CaSRv3.2-R and ERA5) was compared with observations from Sachs Harbour. Results presented in Table 4 showed that CaSRv3.2-F, CaSRv3.2-R and ERA5 all underestimated the frequency of precipitation occurrence, with FBIs smaller than 1. ERA5 had the largest number of missed precipitation days, missing 25 %, compared to 19 % for CaSRv3.2-F and 16 % for CaSRv3.2-R. CaSRv3.2-R had the highest ETS (0.38) and PC (77.5 %).

Total annual precipitation was evaluated using eight years of continuously recorded precipitation. Figure 4a illustrates the results: the average annual precipitation at Sachs Harbour, at 217 mm, was between the ERA5 annual precipitation of 207 mm and the CaSRv3.2-F and CaSRv3.2-R values of 263 and 244 mm, respectively. The comparison highlighted ERA5's underestimation of total precipitation, where the minimum total annual precipitation predicted by the reanalysis was 162 mm for the year 2000, as opposed to 224 mm measured at the LWS for the same year.

https://doi.org/10.5194/egusphere-2026-6730
Preprint. Discussion started: 5 November 2026
© Author(s) 2026. CC BY 4.0 License.

Table 4. Skill scores for daily precipitation occurence: Frequency Bias Index (FBI), Equitable Threat Score (ETS) and proportion of correctly detected events (PC).

	ERA5	CaSRv3.2-R	CaSRv3.2-F
FBI	0.719	0.819	0.882
ETS	0.208	0.383	0.221
PC	0.663	0.775	0.681

Precipitation seasonality was assessed at Sachs Harbour. Corrected daily precipitation data from the LWS were used, covering 33 complete months for each month, represented in Figure 4b. Findings indicated that most precipitation was observed by the LWS between July and October, whereas the distribution of ERA5 precipitation throughout the year was shifted a month earlier, with most precipitation occurring between June and September. CaSRv3.2-R monthly precipitation seemed to capture the seasonality of precipitation observed at the LWS better, while CaSRv3.2-F overestimated precipitation and also presented a shift in precipitation timing similar to ERA5, although smaller in magnitude. The closer agreement between CaSRv3.2-R and Sachs Harbour should be interpreted with caution: precipitation observations from the LWS are assimilated into CaSRv3.2-R, meaning that both dataset are not independent. Additionally, all meteorological reanalyses captured the low accumulation of precipitation between December and April, where the monthly average cumulative precipitation ranged only from 5 to 8 mm.

3.2 Phase Partitioning Methods

All four PPMs, regardless of the meteorological reanalysis with which each was paired, tended to underestimate liquid precipitation (FBI < 1) and overestimate solid precipitation (FBI > 1) in near-freezing periods, as shown in Figure 5. ETS are also very similar between all reanalysis-PPM combinations, where scores range from 0.40, for CaSRv3.2-F with J18, to 0.54, for ERA5 with HP13. While ERA5 consistently produced the highest ETS, B00 led to the largest ETS for a given reanalysis, followed by HP13. Table 5 summarizes the proportion of correctly detected precipitation phase for each pair of meteorological reanalysis and PPM. J18, the only PPM that relies solely on near-surface air temperature, had the lowest proportion of correctly detected events when compared to other PPMs for the same meteorological reanalysis. ERA5 showed the highest proportion of correctly detected precipitation phase across all PPMs, with its highest PC at 0.86 when paired with HP13. In the case of CaSRv3.2-F and CaSRv3.2-R, B00 was the PPM that led to the largest agreement with observed precipitation phase, with 0.83 and 0.84 of correctly detected phases, respectively. Lower skill scores for W19 and HP13 can be attributed to the underestimation of relative humidity, which increased evaporative cooling and contributed to decreasing the resulting liquid precipitation fraction, promoting solid precipitation.

An evaluation of B00 freezing rain predictions at Sachs Harbour revealed that in more than 99 % of freezing rain predictions for CaSRv3.2-R, and on average 98.5 % for CaSRv3.2-F, the same precipitation event was identified as solid for pairings with any other PPM, both through the whole dataset and for near-freezing periods. When validating against LWS weather observations, only 20 % for CaSRv3.2-R (41 events out of 203), and 26 % for CaSRv3.2-F (68 events out of 267), of all freezing

https://doi.org/10.5194/egusphere-2026-6730
Preprint. Discussion started: 5 November 2026
© Author(s) 2026. CC BY 4.0 License.

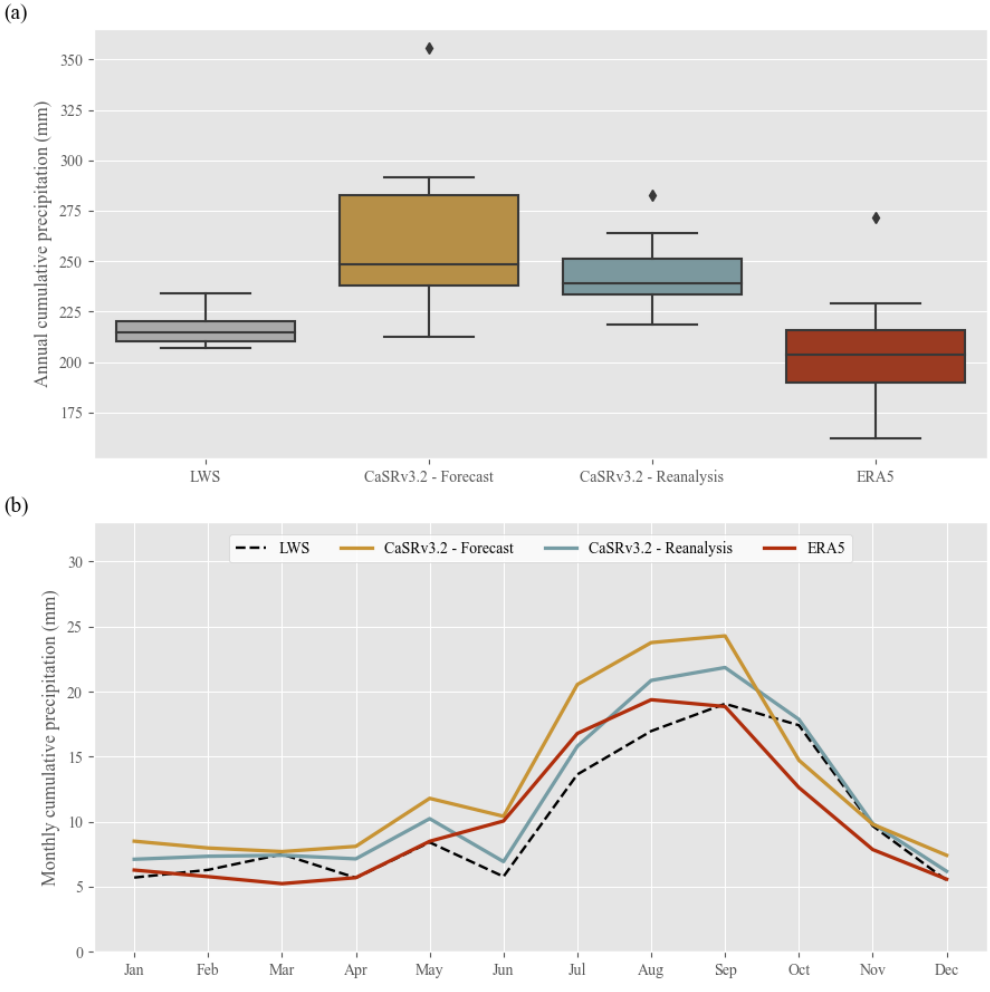


Figure 4. Comparison of cumulative precipitation at Sachs Harbour between 1980 and 2003, where (a) distinguishes total annual precipitation (n per year: 8) and (b) the average of monthly precipitation accumulation (n per month: 33).

https://doi.org/10.5194/egusphere-2026-6730
Preprint. Discussion started: 5 November 2026
© Author(s) 2026. CC BY 4.0 License.

Table 5. Proportion of correctly detected (PC) precipitation phase in near-freezing periods at Sachs Harbour.

	J18	HP13	W19	B00	Average PC
ERA5	0.83	**0.86**	0.85	–	0.85
CaSRv3.2-R	0.80	0.82	0.81	**0.84**	0.82
CaSRv3.2-F	0.80	0.82	0.80	**0.83**	0.81
Average PC	0.81	0.83	0.82	**0.84**	–

rain observations were predicted correctly in near-freezing periods. These predictions happened in 4.7 % of occurrences of all liquid precipitation within near-freezing periods with CaSRv3.2-R, and 5.2 % with CaSRv3.2-F.

The assessment of PPM performance then focused on the ROS event of October 2003 on Banks Island, specifically at Thomsen River, for the period when liquid precipitation is expected near ROS detections. Figure 6a illustrates the precipitation phase partitioning for each meteorological reanalysis paired with the PPM that provided the highest PC. It shows that all reanalyses predicted precipitation between 2 and 6 October, but only B00 partitioned 4.2 mm of it as liquid precipitation. The only difference between CaSRv3.2-F and CaSRv3.2-R was the amount of solid precipitation between 26 September and 10 October 2003, where CaSRv3.2-F predicted 0.9 mm more solid precipitation, consistent with previous results shown in Section 3.1.2 indicating its tendency to overestimate precipitation amounts. As opposed to B00, J18 did not yield any significant amount of liquid precipitation around the 2003 ROS event, while HP13 and W19 captured very small amounts of rainfall (additional results are avaible in Appendix D).

Focusing on the output of B00 in Figure 6b, some of the liquid precipitation was identified as freezing rain and occurred at sub-zero temperatures: the average surface air temperature of CaSRv3.2-R for the freezing rain detection in that window was -0.9°C. Liquid precipitation from CaSRv3.2-R paired with B00 also overlapped with both periods of ROS detection. The second period of ROS detection aligned with rainfall rather than freezing rain, which was driven by above-zero air temperatures at the surface. Above-zero surface air temperatures lasted from October 3 to 5, reaching a maximum of 1.8°C.

3.3 Snowpack modelling

Due to the similarity in performance between ERA5 and CaSRv3.2 for air temperature, wind speed and relative humidity, precipitation quality led the choice for the selected meteorological reanalysis. CaSRv3.2-R had the best fit with the seasonality of precipitation and monthly cumulative precipitation. When paired with B00, it provided a high proportion of correctly detected occurrence of precipitation events and was able to predict liquid precipitation aligned with the positive ROS detections from remote sensing at Thomsen River in October 2003. CasRv3.2-R coupled with B00 detected a total of 4.16 mm of rainfall between 19 September and 10 October 2003 at Thomsen River, accompanied by above-zero temperatures. As a result, this combination was selected to run the snowpack model.

https://doi.org/10.5194/egusphere-2026-6730
Preprint. Discussion started: 5 November 2026
© Author(s) 2026. CC BY 4.0 License.

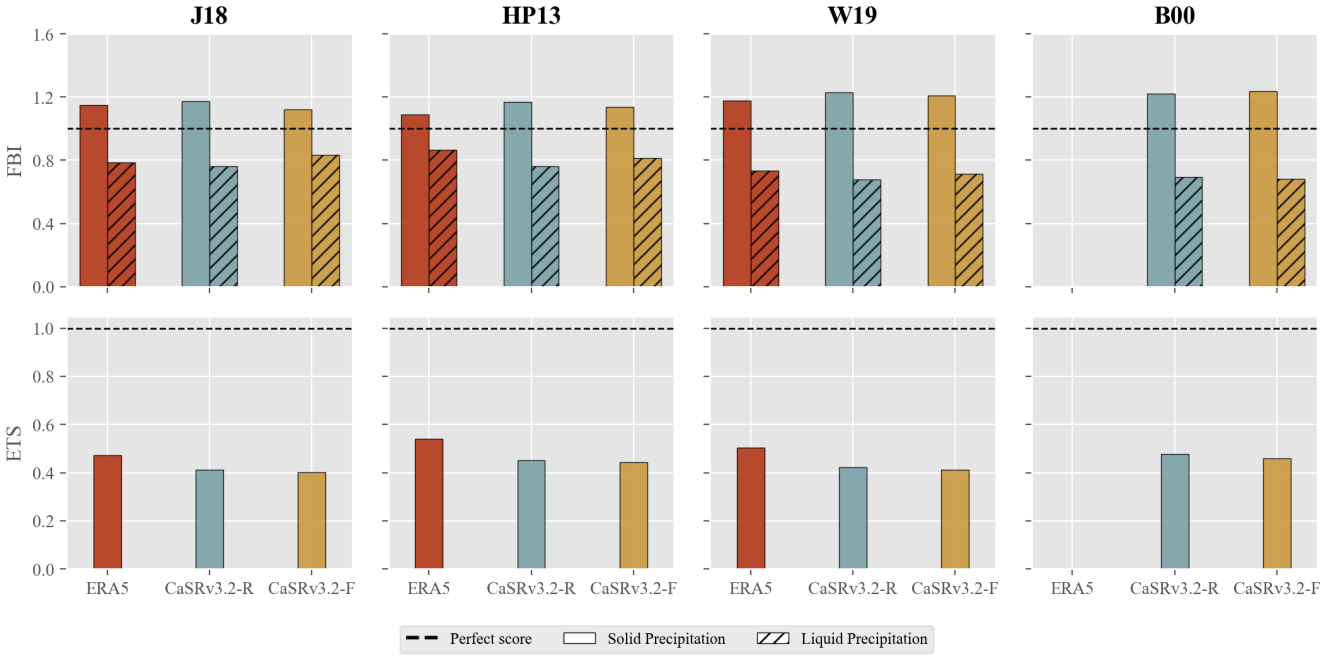


Figure 5. FBI and ETS for near-freezing period precipitation phase detection skill of each meteorological reanalysis and PPM pairing. Perfect scores for both FBI and ETS is 1. The ETS is shown only for solid precipitation because the ratio is the same for both solid and liquid precipitation.

3.3.1 SVS2-Crocus ensemble

The output of the ensemble run for the ROS event of 2003 at Thomsen River revealed that 80 out of the 108 simulations had created a locked pasture by the end of October 2003, as shown in Figure 7. Across those 80 simulated locked pastures, the average density of the locked pasture snow layers was 398 kg m^{-3} (ranging from 353 to 459 kg m^{-3}), with an average thickness of 4.1 cm (ranging from 3.3 to 4.3 cm). Figure 8 illustrates the distribution of density of the basal 20 mm of the snowpack. The driving parameter of locked pasture simulation was the water holding capacity, where basal density distributions have smaller ranges and each option yields different results. SPK and B92 consistently led to locked pastures, regardless of their combination with other parameters due to their ability to hold more water than B02 and O04. Beyond water holding capacity, other parametrizations that most frequently resulted in locked pastures were those that increased the effect of wind speed: R21F (wind packing), which integrated both an increase in maximum snow density and an enhanced wind effect, R21 (falling snow density), which corresponds to the highest increase in the effect of wind speed, and S14 (snow compaction), which increases densification within the first 48-h after snowfall.

A closer look at one of the snowpack simulation that formed a locked pasture for the winter of 2003–2004 (water holding capacity: B92, snow compaction: S14, falling snow density: R21 and wind packing: R21F, shown in Figure 9) revealed that

https://doi.org/10.5194/egusphere-2026-6730
Preprint. Discussion started: 5 November 2026
© Author(s) 2026. CC BY 4.0 License.

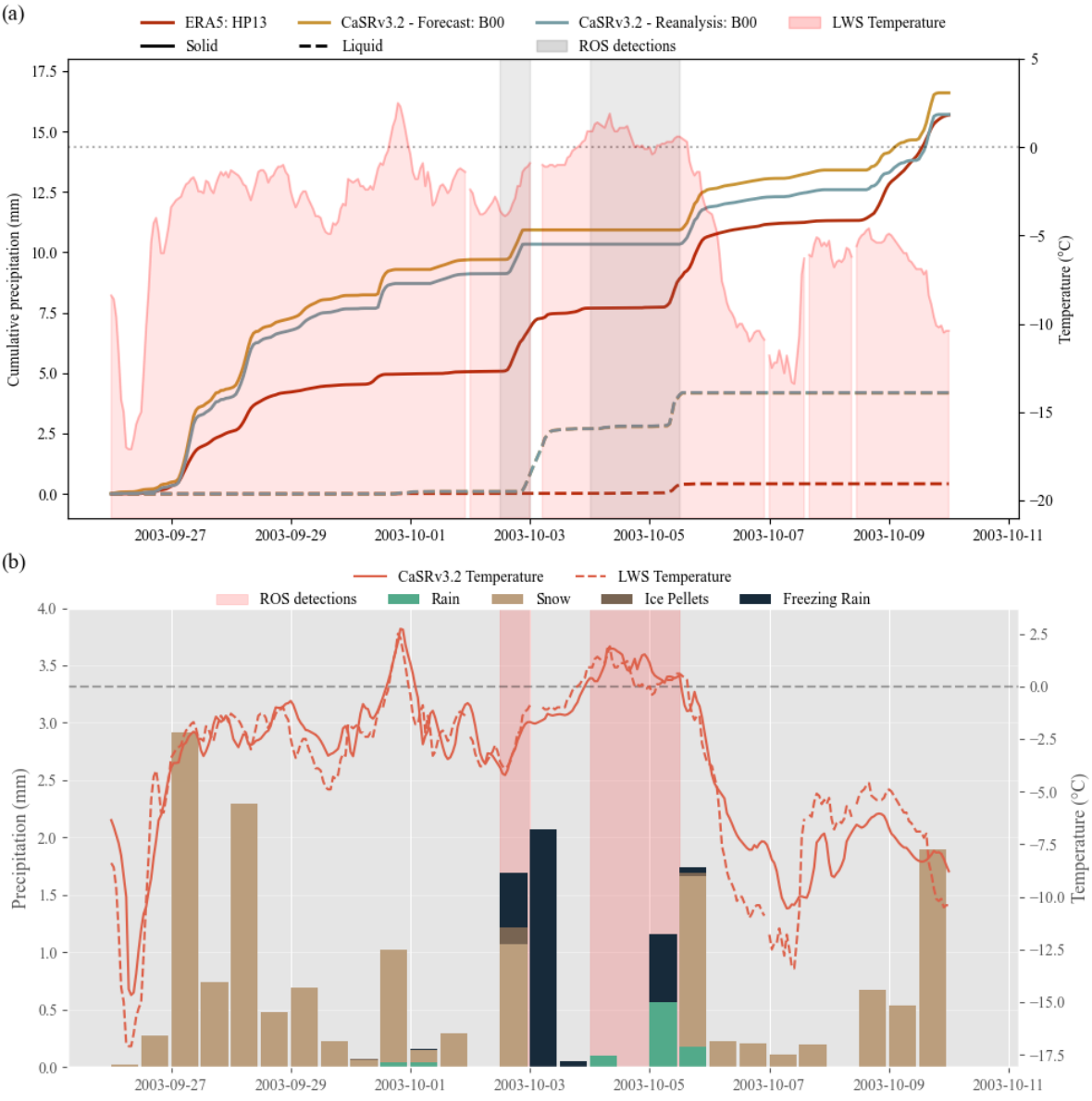


Figure 6. Comparison of solid and liquid precipitation accumulation around the rain-on-snow event of October 2003 at Thomsen River. (a) Phase partitioning coupling ERA5 with HP13 and B00 with both CaSRv3.2-R and CaSRv3.2-F. (b) CaSRv3.2-R paired with B00 precipitation phase partition around the ROS event of October 2003. See Appendix D for all reanalysis-PPM pairing precipitation phase partitioning around the ROS event.

https://doi.org/10.5194/egusphere-2026-6730
Preprint. Discussion started: 5 November 2026
© Author(s) 2026. CC BY 4.0 License.

freezing rain occurred around the first ROS detection, creating a thin ice layer on the surface of the snowpack, which then melted over the second detection of ROS. The melt event was identified in the insets of Figure 9 through the decrease in snow depth, but also because of the presence of liquid water and close-to-zero temperatures through the entire snowpack, indicating a short ripening of the snow cover. Liquid precipitation also contributed to the ripening of the snowpack during the warm event. Cold weather then refroze the snowpack, creating a 4 cm thick basal layer of 447 kg m^{-3} composed of melt forms and faceted crystals of high strength Fierz et al. (2009) that would have prevented ungulates from foraging until May 2004 (Figure 9).

The cold simulation in Figure 10a, isolating the freezing rain event, prevented the ripening of the snowpack. Out of 108 runs of the cold ensemble, only one produced a locked pasture, with an average basal density of 358 kg m^{-3} and a thickness of 6.9 cm. The only combination of parameters that led to the formation of a locked pasture was B02 (water holding capacity), S14 (snow compaction), R21 (falling snow density) and R21F (wind packing). In the vast majority of simulations, freezing rain created an ice crust at the surface of the snowpack, which then appeared to merge with surrounding snow layers before quickly disappearing (Figure 10a).

ROS events only occurs if the air temperature is warm enough for precipitation particles to melt, which means that ROS events are often paired with above-zero temperatures that contribute to melting the snowpack. The no-rain simulations allowed to isolate the warm event and led to the formation of a locked pasture in 55.6 % of the runs (Figure 10b). On average, the recreated locked pasture had a density of 383 kg m^{-3} and a thickness of 4 cm. Similar patterns in parametrizations were observed both in the ensemble and the no-rain simulations: common parametrizations that simulated a locked pasture included the water holding capacity B92 and SPK, wind packing R21F, snow compaction S14 and falling snow density R21. Results of the no-rain simulation displayed in Figure 10b indicated two important melt events (1 and 4 October 2003) that contributed to the densification of the basal layer of the snowpack, which could be identified through a sudden increase in dense snow probability that spanned from the surface of the snowpack to underlying layers.

3.3.2 Historical locked pastures

A long-term snow ensemble simulation at Thomsen River revealed a stratigraphy in which historical locked pastures were identified (Figure 11). In 2003 and 2008, 73 and 58 % of simulations respectively agreed on a basal snow layer denser than 350 kg m^{-3} and thicker than 20 mm by the end of October. Both events overlapped with freezing rain, according to CaSRv3.2-R, with a total of 3.3 mm of freezing rain in 2003 between the first snow accumulation in SVS2-Crocus on 13 September and 31 October and 6.0 mm for the 2008 event between 22 September and 31 October. Both potential locked pastures overlapped with four and one detections of ROS at Thomsen River for 2003 and 2008 respectively.

In the case of the snow stratigraphy in 1988, 1990 and 1998, the probability of a locked pasture formation is lower, between 27 and 40 %, but each instance overlaps with either remote sensing detections of ROS (for 1988 and 1998) or severe ROS conditions on Banks Island that led to ungulate die-offs (for 1990). Focusing on 1988, all simulations of the ensemble formed a locked pasture around the ROS detection, which aligned with liquid precipitation, but due to snow layers merging within the model, the dense basal layer was lost in a majority of simulations. For 1998, the ROS detection happened eight days before the snow onset in SVS2-Crocus and the high density layer that we observe in the output is due to other physical processes, such

https://doi.org/10.5194/egusphere-2026-6730
Preprint. Discussion started: 5 November 2026
© Author(s) 2026. CC BY 4.0 License.

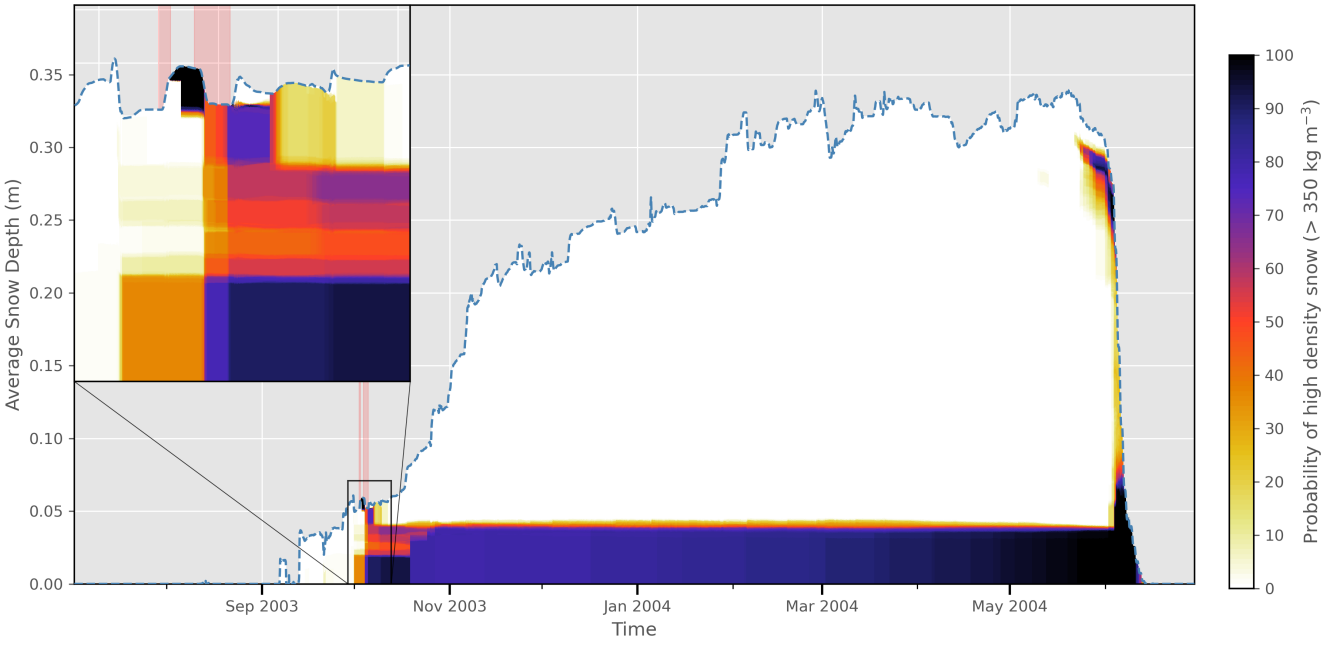


Figure 7. Location of snow layers with densities above 350 kg m^{-3} for all 108 SVS2-Crocus ensemble simulations, normalized across average winter snow depth. Highlighted in red are the positive detections of ROS (Langlois et al., 2026)

as snow compaction, that increased the density of the basal snow layer past the 350 kg m $^{-3}$ threshold. Finally, in 1990, no ROS was remotely detected, but CaSRv3.2-R predicted a total of 1.1 mm of liquid precipitation between 22 and 25 September, as well as above-freezing temperatures reaching up to 2.5°C, while the snowpack was still very shallow (3̃.5 cm), forming a denser basal layer that increased in density through snow compaction. It is important to note that the severe ROS events linked to die-offs are reported across Banks Island, not specifically at Thomsen River, and therefore are not intended to explain the stratigraphy presented in Figure 11.

Figure 11 also shows that in 1996, ROS was detected, but no locked pasture was simulated, whilst in 2015, the opposite happened. In 1996, the ROS detection happened during a five-day period where temperatures were oscillating around 0°C and during which a total of 30.6 mm of liquid precipitation happened. The snowpack simulations of SVS2-Crocus featured a complete melt of the snow cover over this period, leading to a locked pasture-free snowpack that accumulated again soon after the liquid precipitation. For 2015, SVS2-Crocus snow onset happened on 20 September, while the NOAA snow onset was on 11 October, meaning that any polarized gradient ratio (GRP) lower than the -2 threshold between both dates was discarded in the original dataset due to the lack of snow cover. An evaluation of the historical ROS dataset indicated that a ROS detection was removed on 30 September 2015 (GRP = -3.93). The positive ROS detection overlapped with a small rainfall (0.2 mm) and above-freezing temperatures up to 2.3° C that ripened the snowpack before it refroze and got compacted as a result of the following snowfall, which created the low probability locked pasture in snowpack simulations.

https://doi.org/10.5194/egusphere-2026-6730
Preprint. Discussion started: 5 November 2026
© Author(s) 2026. CC BY 4.0 License.

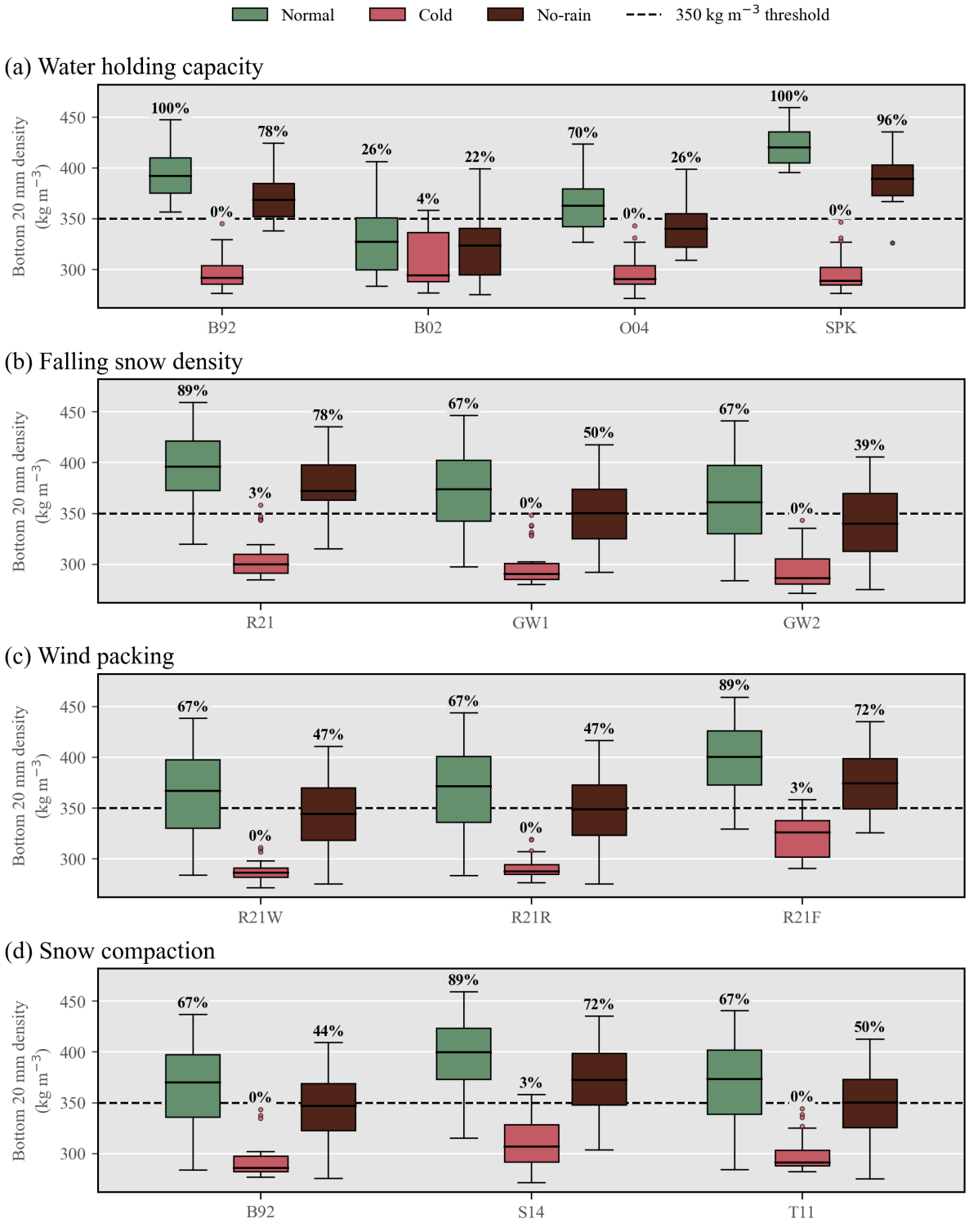


Figure 8. Distribution of the bottom 20 mm density for each physical processes of the three ensemble simulations (normal, cold & no-rain), with the percentage of simulated locked pastures above each box.

https://doi.org/10.5194/egusphere-2026-6730
Preprint. Discussion started: 5 November 2026
© Author(s) 2026. CC BY 4.0 License.

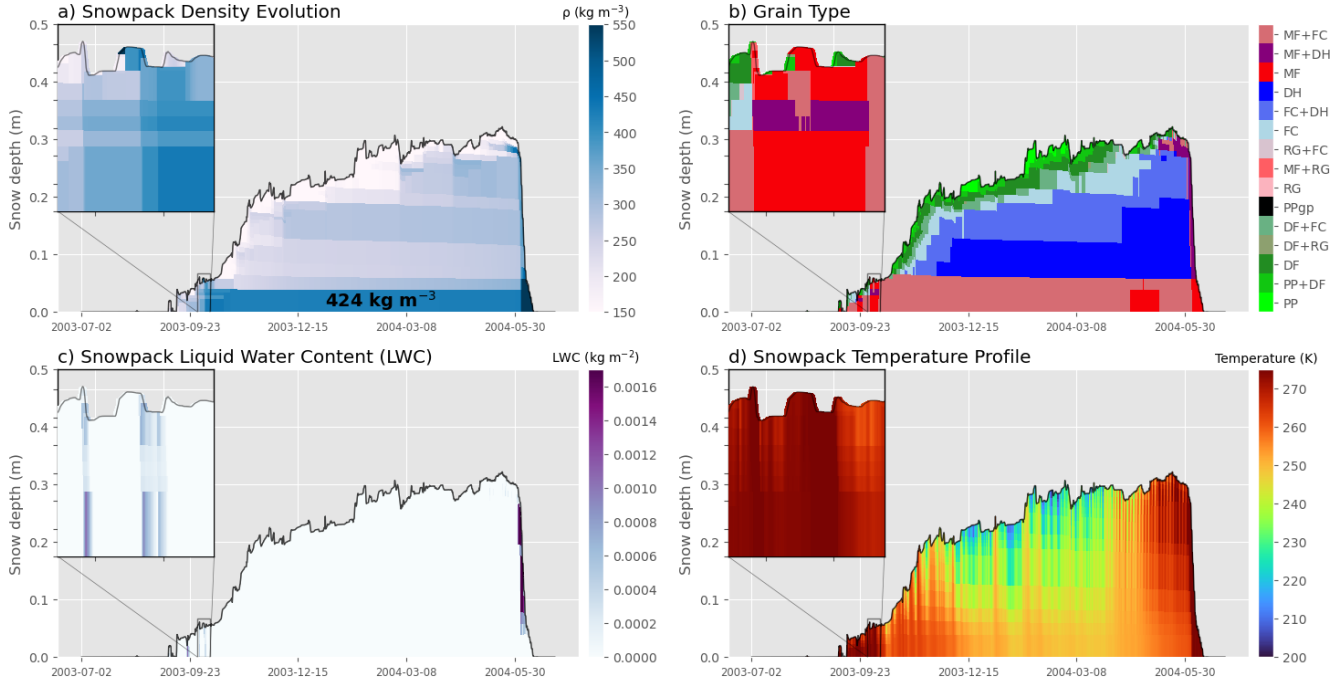


Figure 9. Details of the Crocus-SVS2 simulation at Thomsen River with CaSRv3.2 paired with B00 for the winter 2003-04. Highlighted in red are the positive detections of ROS (Langlois et al., 2026). From left to right, top to bottom: snowpack density evolution, grain type, liquid water content of the snowpack & temperature profile of the snowpack. Parameters of the simulation shown: B92 (water holding capacity), S14 (snow compaction), R21 (falling snow density) and R21F (wind packing). A full description of grain types can be found in Appendix E

https://doi.org/10.5194/egusphere-2026-6730
Preprint. Discussion started: 5 November 2026
© Author(s) 2026. CC BY 4.0 License.

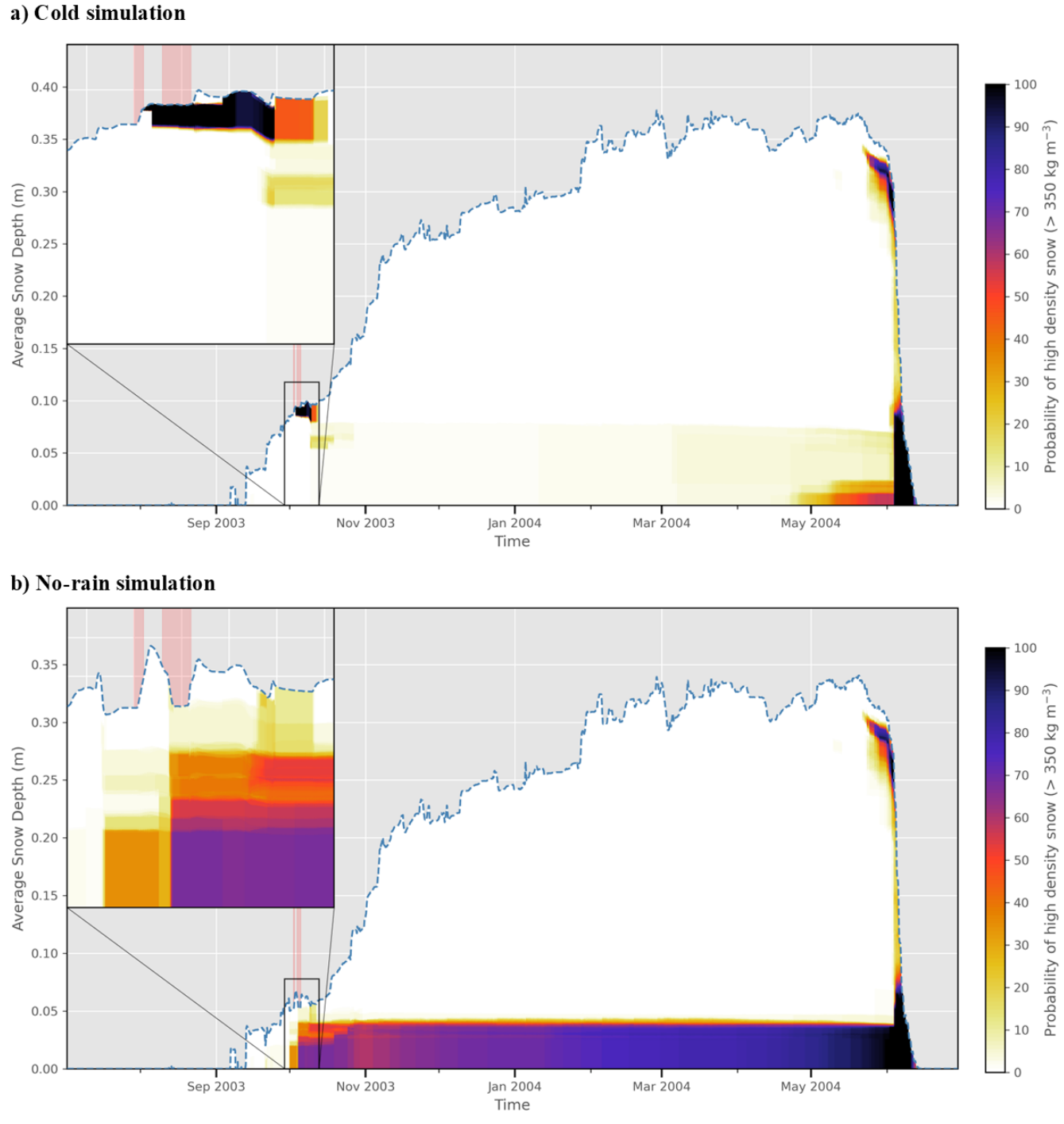


Figure 10. Location of snow layers with densities above 350 kg m^{-3} for all SVS2-Crocus ensemble simulations, normalized across average winter snow depth, for (a) the cold simulation and (b) the no-rain simulation. Details about these simulations are given in Section 2.5

https://doi.org/10.5194/egusphere-2026-6730
Preprint. Discussion started: 5 November 2026
© Author(s) 2026. CC BY 4.0 License.

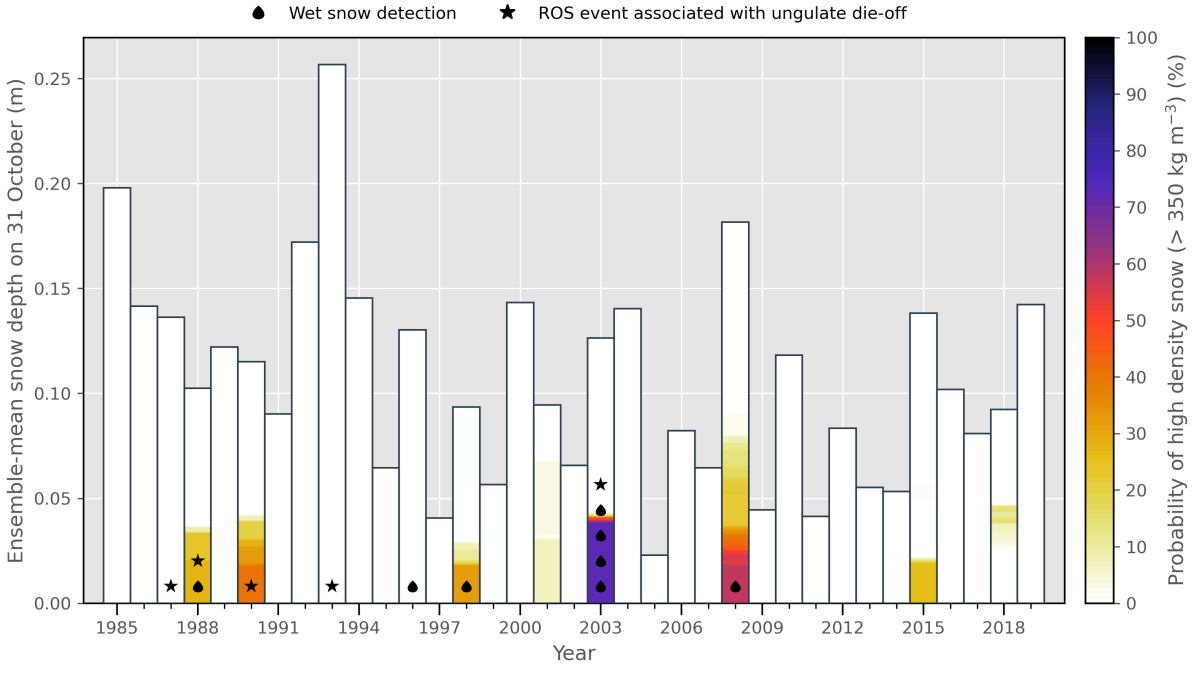


Figure 11. Time series of snowpack density on 31 October each year between 1985 and 2020 from all SVS2-Crocus ensemble simulations, overlaid with the number of positive ROS detections for the winter season from Langlois et al. (2026). Stars indicate years associated with ungulate die-offs due to ROS events on Banks Island in the literature (Table 3 of Langlois et al., 2026).

https://doi.org/10.5194/egusphere-2026-6730
Preprint. Discussion started: 5 November 2026
© Author(s) 2026. CC BY 4.0 License.

4 Discussion

Locked pastures as a result of ROS events were simulated with SVS2-Crocus, demonstrating that current snowpack models contain physical equations are able to represent this phenomenon. 74 % of simulations recreated the locked pasture reported by the Sachs Harbour community (Rennert et al., 2009). The ensemble approach allows challenges in Arctic snow modelling to be tackled by taking advantage of different representations of processes and assessing the results as an indicator of probability (Menard et al., 2024). Combining parameters responsible for water percolation and snow density therefore provides a good estimate of locked pasture probability, and by extension, of the risk this poses to foraging ungulates.

The ensemble-approach also allows to compensate for Arctic physical snow processes that are not well captured by the snowpack model, where various parametrizations may compensate for this bias. Several studies have shown that a limitation of the snowpack models, when applied to Arctic environments, is the underestimation of wind-induced compaction (Barrere et al., 2017; Royer et al., 2021b; Lackner et al., 2022). Li and Pomeroy (1997) have demonstrated that the wind speed threshold for dry snow transport is, on average, 7.7 m s^{-1}, which corresponds to the measured wind speed where the disagreement starts to get larger between models and observations in Figure 3. Such a bias in wind speed is likely to affect the snowpack model's ability to densify snow as a consequence of wind speed through wind packing or falling snow density and model outputs confirmed that locked pasture simulations were driven by Arctic schemes that increased the effect of wind packing (Woolley et al., 2024). Additional simulations revealed that melt events, driven by above-zero surface temperatures at the beginning of the winter without any liquid precipitation, can lead to the formation of a locked pasture, but the addition of rainfall increases the risks considerably. Literature support this claim (Langlois et al., 2026; Vickers et al., 2022; Bartsch et al., 2010), showcasing the reliability of the outputs of the simulation ensemble and the potential of using snowpack models to better understand meteorological conditions leading to locked pastures.

The long term simulation correctly identified with high probability (58 to 74 %) two locked pastures that have been detected remotely. Simulations with lower probability of locked pastures (27 to 40 %) identified three years where the snow conditions could have prevented foraging activities, where two of those were linked to ungulate die-offs as a result of ROS events in 1988 and 1990 and the third one corresponded to a ROS detection in 1998. Detection of ROS in 1996 did not correlate with any simulated locked pasture or die-off, but did correspond to a major ROS year on Banks Island according to Langlois et al. (2026). While the meteorological driving data predicted a large amount of liquid precipitation around the 1996 ROS detection, the snow cover in simulations fully melted during this period and only started accumulating after the liquid precipitation. As for the 2015 dense basal layer (25 % probability), a ROS detection was removed from the dataset because of the date of the snow onset within the NOAA snow cover dataset was three weeks later than the SVS2-Crocus simulations, where the positive ROS detection overlaps with the simulated snow onset. Lower probability of locked pastures following a ROS event is consistent with the findings of Larter and Nagy (1994), who have observed that not all ROS events lead to a locked pasture and heterogeneity of the resulting snow stratigraphy is to be expected. In remote Arctic regions where very few LWS are located, confirmation of the presence of a locked pasture or a ROS event are hard to obtain and make validation particularly dependent on Inuit knowledge. Studies that leverage Inuit Knowledge to better understand changing winter conditions, extreme weather

https://doi.org/10.5194/egusphere-2026-6730
Preprint. Discussion started: 5 November 2026
© Author(s) 2026. CC BY 4.0 License.

events and their consequences, such as Langlois et al. (2026), Rasmus et al. (2020, 2018) or Markkula et al. (2025) are crucial to understanding the impacts of climate warming on the Arctic ecosystem.

For a meteorological reanalysis to predict rain around the freezing point, the PPM should rely on atmospheric temperature profile rather than near-surface variables, especially in coastal areas. Pernov et al. (2024) showed that coastal locations in the Arctic were subject to larger errors in relative humidity than sites situated further inland. PPMs are impacted by biases in surface air temperature and humidity of the reanalysis with which it is paired. Underestimated relative humidity led both reanalyses to overestimate solid precipitation in near-freezing conditions, reducing the chances of capturing ROS events, whilst B00, which relies on the vertical air profile, provided better accuracy. W19 was expected to perform better than HP13, since the latter equation was calibrated in the Canadian Rockies, as opposed to a range of different climates across the United States like W19 (Harder and Pomeroy, 2013; Wang et al., 2019), but similar agreement percentages were observed between both calculation methods, which can be explained by the low accuracy in relative humidity predictions. Results suggest that J18, an optimized temperature threshold, can be a good alternative if relative humidity is not available or accurate, as also shown by Leroux et al. (2023). Nonetheless, B00 was the only PPM that predicted liquid precipitation within the expected timing of the ROS event, because it relies on a vertical air temperature profile that allows for predicting liquid precipitation at low surface air temperatures, leading to occurrences of freezing rain, as observed in October 2003 at Thomsen River. This advantage, however, is only meaningful if the underlying meteorological reanalysis itself captures precipitation accurately, which is not guaranteed across all products.

It is crucial for meteorological forcing data to identify ROS events in late autumn to simulate locked pasture formation. Local reanalyses, such as CaSRv3.2, are more accurate than global reanalyses in terms of precipitation, nevertheless, in this case, it is not true for other meteorological variables (2 m air temperature, wind speed and 2 m relative humidity). To identify ROS events in late autumn that are responsible for locked pastures, accuracy in precipitation timing is crucial. ERA5 displayed a clear underestimation precipitation in October, which overlaps with the period where critical ROS events tend to happen (Hansen et al., 2014; Laptander et al., 2024; Serreze et al., 2021). The precipitation seasonality bias of ERA5 at Sachs Harbour agrees with the misalignment in Arctic precipitation observed by Obarein and Lee (2025). Assimilation of corrected LWS precipitation records in CaSRv3.2-R (Khedhaouiria et al., 2026) allowed the resulting precipitation product to better capture precipitation timing, overcoming ERA5 coastal modelling challenges (Hersbach et al., 2020). Evaluation of monthly precipitation amounts highlighted biases in meteorological reanalyses precipitation products that would considerably limit their ability to capture critical ROS events.

5 Conclusions

Current snowpack models contain physical equations capable of simulating locked pastures. To demonstrate this, the ability of ERA5 and CaSRv3.2 to capture key elements of ROS events that lead to locked pastures, defined as a basal snow layer of at least 20 mm and with a density greater than 350 kg m $^{-3}$, was assessed, and the capacity of SVS2-Crocus to recreate locked pasture stratigraphy following a ROS event was evaluated. CaSRv3.2 captured the seasonality of precipitation at Sachs Harbour

https://doi.org/10.5194/egusphere-2026-6730
Preprint. Discussion started: 5 November 2026
© Author(s) 2026. CC BY 4.0 License.

more accurately than ERA5, highlighting that the choice of meteorological reanalysis and phase partitioning method is key to identifying ROS in the Arctic. Validating against a well-documented ROS event and then against a long-term simulation compared to a remote sensing record, the ensemble approach based on water percolation and density-related schemes was able to indicate locked pasture likelihood and help identify the physical and meteorological processes driving it. Small amounts of liquid precipitation, or even a melt event alone, can have catastrophic consequences for local fauna, and historical simulations correctly simulated 4 of 5 past locked pastures, including two linked to ungulate die-offs.

Reported locked pastures were successfully simulated, demonstrating that the right combination between a meteorological reanalysis and a PPM is sufficient to drive snow simulations and provide a reliable indication of snow stratigraphy across the Canadian Arctic Archipelago. Linking meteorological drivers to the formation of locked pastures helps disentangle the contribution of ROS events to past ungulate population declines of muskoxen and Peary caribou. Combined with Inuit knowledge, the present method establishes a foundation for spatially distributed applications across the Canadian Arctic, allowing identification or even prediction of suitable winter habitats for caribou and muskoxen. Modelling of locked pastures could support wildlife management decisions and, in turn, help mitigate the consequences of ROS events for ungulate populations and the Inuit communities that rely on them for food, economy and traditional practices.

https://doi.org/10.5194/egusphere-2026-6730
Preprint. Discussion started: 5 November 2026
© Author(s) 2026. CC BY 4.0 License.

Appendix A: FBI, ETS & PC precipitation scores

Table A1 is the 2×2 contingency table used as a basis for the calculation of the Frequency Bias Index (FBI), the Equitable Threat Score (ETS) and the proportion of correctly identified events (PC).

Table A1. A standard 2×2 contingency table for binary event verification.

		Observations	
		True	False
Forecast	True	a (true positive)	b (false positive)
	False	c (false negative)	d (true negative)

The FBI is the ratio of the total number of forecasted events to the total number of observed events. It provides indications of the bias of a forecast for the frequency of an event. An FBI score ranges between 0 and ∞, where a value lower than 1 corresponds to an underestimation of the event, a value greater than 1 indicates an overestimation and the perfect score is 1.

$$FBI = \frac{a+b}{a+c} \tag{A1}$$

The ETS represents the skill of a forecast relative to chance. ETS ranges between $-1/3$ and 1, where a negative value is interpreted as worse predictions than chance and 1 is the perfect score.

$$ETS = \frac{a-h_r}{a+b+c-h_r} \tag{A2}$$

where $h_r = \frac{(a+b)(a+c)}{a+b+c+d}$ represents true positives expected by chance.

The PC, proportion of correctly detected events, corresponds to the sum of true positives and true negatives, divided by the total amount of all events. Resulting score is between 0 and 1, where 1 is the perfect score. The equation below was used to calculate the PC throughout the analysis:

$$PC = \frac{a+d}{a+b+c+d} \tag{A3}$$

https://doi.org/10.5194/egusphere-2026-6730
Preprint. Discussion started: 5 November 2026
© Author(s) 2026. CC BY 4.0 License.

Appendix B: SVS2-Crocus parameters for Thomsen River

Table B1 describes the content of the soil layers used in SVS2-Crocus for Thomsen River. Not shown in the table are an additional six layers of soil that have the same parameters as layer 6. The next six layers have the following thicknesses (from layer 7 to 12): 0.40, 0.60, 1.00, 1.50, 2.50 and 3.50 m. The underlying permafrost temperature was set to 264.8 K. The polar vegetation height was set to 0 m, but the specified canopy was identified as 100% tundra with a roughness height of 2.5 cm. Specific snow parameters were set according to Table B2.

Table B1. Soil content description of SVS2-Crocus for Thomsen River.

Soil layer	**1**	**2**	**3**	**4**	**5**	**6**
Thickness (m)	0.05	0.05	0.10	0.10	0.20	0.30
Sand (%)	58.50	58.50	62.40	65.40	66.70	40.90
Clay (%)	12.50	12.50	12.50	10.55	10.92	19.70
Soil organic content (%)	9.60	9.60	6.20	2.48	2.44	2.93
Water volume content (m^3m^{-3})	0.14	0.17	0.18	0.20	0.21	0.19
Ice volume content (m^3m^{-3})	0.00	0.00	0.00	0.00	0.00	0.50
Soil temperature (K)	284	282	280	280	278	270

Table B2. Multilayer snowpack scheme parameters used for the SVS2-Crocus simulations. Setting descriptions can be found in Vionnet et al. (2012), Lafaysse et al. (2017) and Woolley et al. (2024).

Variable	**Setting**
Number of snow layers	24
Albedo evolution (days)	495
Mass loss from blowing snow	True
Metamorphism scheme	B21
Radiative transfer scheme	S97
Turbulent fluxes	DEF
Water holding capacity	SPK | B92 | B02 | O04
Compaction scheme	B92 | T11 | S14
Falling snow density	R21 | GW1 | GW2
wind packing scheme	R21W | R21F | R21R

https://doi.org/10.5194/egusphere-2026-6730
Preprint. Discussion started: 5 November 2026
© Author(s) 2026. CC BY 4.0 License.

Appendix C: Dataset size

Table C1 summarizes the size and range of the overlap between the LWS dataset and each meteorological reanalysis over their full range and for the near-freezing periods sampling. Near-freezing periods correspond to the sample where the LWS surface air temperature is located between -5 and 5°C. On average, they represent about 24.8% of the data available. The near-freezing periods + 5°C threshold sample is issued from the near-freezing periods with an additional threshold of 5°C for the maximum tolerated difference between the reanalysis and LWS air temperature.

Table C1. Overview of the dataset size used for assessing the performance of meteorological reanalyses at each LWS. *n* corresponds to the number of hourly data that was both available at the LWS and in the meteorological reanalysis. Additional details about the table can be found in Appendix B.

LWS	Meteorological reanalysis	Start date	End date	Full dataset (n)	Near-freezing periods (n)	Near-freezing periods + 5° C threshold (n)
Sachs Harbour	ERA5	01/09/1980	31/07/2020	143696	38653	38601
	CaSRv3.2	01/09/1980	02/07/2020	142997	38259	37859
Nangmagvik Lake	ERA5	21/08/1996	31/07/2020	142972	37603	37560
	CaSRv3.2	21/08/1996	09/08/2018	142538	37334	36974
Thomsen River	ERA5	26/07/1997	31/07/2020	149882	32116	32077
	CaSRv3.2	26/07/1997	02/07/2020	149193	32002	31707
Average				145213	35995	35796

https://doi.org/10.5194/egusphere-2026-6730
Preprint. Discussion started: 5 November 2026
© Author(s) 2026. CC BY 4.0 License.

Appendix D: Meteorological reanalysis & PPM for Thomsen River

Figure D1 displays all of the reanalysis-PPM pairing for Thomsen River between 26 September and 10 October 2003.

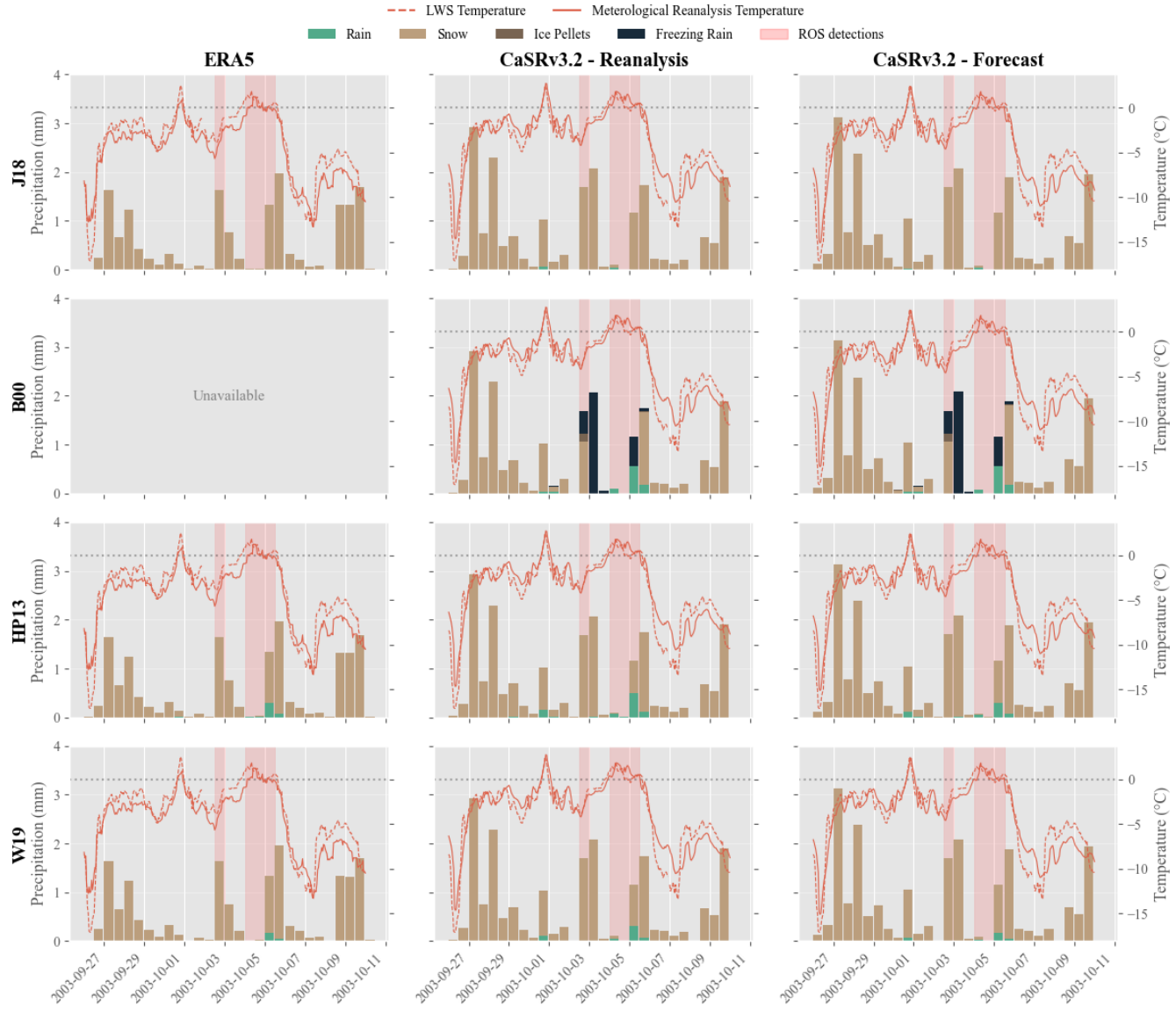


Figure D1. Comparison of solid and liquid precipitation 12-hours accumulation around the rain-on-snow event of October 2003 at Thomsen River for each combination of meteorological reanalysis and PPM.

https://doi.org/10.5194/egusphere-2026-6730
Preprint. Discussion started: 5 November 2026
© Author(s) 2026. CC BY 4.0 License.

Appendix E: Description of the snow grain types

Detailed description of the grain types classified by SVS2-Crocus as identified by their code in Figure 9, as described by Fierz et al. (2009).

https://doi.org/10.5194/egusphere-2026-6730
Preprint. Discussion started: 5 November 2026
© Author(s) 2026. CC BY 4.0 License.

Table E1. SVS2-Crocus snow grain type description as classified by Fierz et al. (2009)

Code	Classification name	Physical process	Variations
DF (/)	Decomposing and fragmented precipitation particles	Precipitation particles fragmented due to wind or decomposed because of reduced surface free energy.	DF_{dc}: Partly decomposed precipitation particles DF_{bk}: Wind-broken precipitation particles
DH ($\wedge$)	Depth hoar	Grain-to-grain vapour diffusion driven by large temperature gradient, i.e., excess vapour density is well above critical value for kinetic growth.	DH_{cp}: Hollow cups DH_{pr}: Hollow prisms DH_{ch}: Chains of depth hoar DH_{la}: Large striated crystals DH_{xr}: Rounding depth hoar
FC ($\square$)	Faceted crystals	Grain-to-grain vapour diffusion driven by large enough temperature gradient, i.e., excess vapour density is above critical value for kinetic growth	FC_{so}: Solid faceted particles FC_{sf}: Near surface faceted particles FC_{xr}: Rounding faceted particles
MF ($\circ$)	Melt forms	Either wet snow or re-frozen snow.	MF_{cl}: Clustered rounded grains MF_{pc}: Rounded polycrystals MF_{sl}: Slush MF_{cr}: Melt-freeze crust
PP ($+$)	Precipitation particles	Growth in atmospheric conditions of a specific water vapour and air temperature.	PP_{co}: Columns PP_{nd}: Needles PP_{pl}: Plates PP_{sd}: Stellars, dendrites PP_{ir}: Irregular crystals PP_{gp}: Graupel PP_{hl}: Hail PP_{ip}: Ice pellets PP_{rm}: Rime
RG ($\bullet$)	Rounded grains	Decrease specific surface area from temperature gradients or saltation by wind.	RG_{sr}: Small rounded particles RG_{lr}: Large rounded particles RG_{wp}: Wind packed RG_{xf}: Faceted rounded particles

https://doi.org/10.5194/egusphere-2026-6730
Preprint. Discussion started: 5 November 2026
© Author(s) 2026. CC BY 4.0 License.

Code and data availability. Codes to process the data and reproduce the figures, the modelling parameters used with SVS2-Crocus and links to datasets used in this study are openly available at: https://github.com/erika-boisvert/Simulating-locked-pastures-in-snow-from-Arctic-rain-events_Supplements. Due to their large size, the SVS2-Crocus simulation output files are not hosted in a public repository, but are available from the corresponding author (erika.boisvert-vigneault@northumbria.ac.uk) upon request.

Author contributions. E. Boisvert-Vigneault led the research, completed the analyses, snow simulations and drafted the manuscript. V. Vionnet and N. Leroux extracted the meteorological dataset and provided support and scientific input for meteorological analyses and snow simulations. J.-A. Langlois provided the historical remote sensing dataset of rain-on-snow for Banks Island. M. Sandells, N. Rutter, A. Langlois and H. Bloomfield provided scientific input and supervised the project. All authors reviewed and contributed to the paper.

Competing interests. At least one of the (co-)authors is a member of the editorial board of *The Cryosphere*. The authors also have no other competing interests to declare.

Disclaimer. Copernicus Publications remains neutral with regard to jurisdictional claims made in the text, published maps, institutional affiliations, or any other geographical representation in this paper. While Copernicus Publications makes every effort to include appropriate place names, the final responsibility lies with the authors. Views expressed in the text are those of the authors and do not necessarily reflect the views of the publisher.

Acknowledgements. The authors thank Environment and Climate Change Canada (ECCC) Meteorological Research Division for allowing them to use their servers to run the snow simulations. The authors also acknowledge ECMWF and ECCC for their support concerning publicly available datasets. Claude (https://claude.ai) was used to assist with the development of Python code for optimizing data processing and simulation output figures in this study. All content was originally created, reviewed and edited by the authors. For the purpose of open access, the author has applied a Creative Commons Attribution (CC BY) licence to any Author Accepted Manuscript (AAM) version arising from this submission.

Financial support. This research has been supported by the Natural Environment Research Council (grant no. NE/S007512/1).

Review statement. The review statement will be added by Copernicus Publications listing the handling editor as well as all contributing referees according to their status, anonymous or identified.

https://doi.org/10.5194/egusphere-2026-6730
Preprint. Discussion started: 5 November 2026
© Author(s) 2026. CC BY 4.0 License.

References

Barrere, M., Domine, F., Decharme, B., Morin, S., Vionnet, V., and Lafaysse, M.: Evaluating the performance of coupled snow–soil models in SURFEXv8 to simulate the permafrost thermal regime at a high Arctic site, Geoscientific Model Development, 10, 3461–3479, https://doi.org/10.5194/gmd-10-3461-2017, 2017.

Bartelt, P. and Lehning, M.: A physical SNOWPACK model for the Swiss avalanche warning: Part I: numerical model, Cold Regions Science and Technology, 35, 123–145, https://doi.org/10.1016/S0165-232X(02)00074-5, 2002.

Bartsch, A., Kumpula, T., Forbes, B. C., and Stammler, F.: Detection of snow surface thawing and refreezing in the Eurasian Arctic with QuikSCAT: implications for reindeer herding, Ecological Applications, 20, 2346–2358, https://doi.org/10.1890/09-1927.1, _eprint: https://onlinelibrary.wiley.com/doi/pdf/10.1890/09-1927.1, 2010.

Boisvert, L. N., Webster, M. A., Parker, C. L., and Forbes, R. M.: Rainy Days in the Arctic, Journal of Climate, 36, 6855–6878, https://doi.org/10.1175/JCLI-D-22-0428.1, 2023.

Bonsoms, J., López-Moreno, J. I., Alonso-González, E., Deschamps-Berger, C., and Oliva, M.: Rain-on-snow responses to warmer Pyrenees: a sensitivity analysis using a physically based snow hydrological model, Natural Hazards and Earth System Sciences, 24, 245–264, https://doi.org/10.5194/nhess-24-245-2024, 2024.

Boone, A.: Description du Schema de Neige ISBA-ES (Explicit Snow), Tech. rep., Centre National de Recherches Météorologiques, Météo-France, Toulouse, France, 2002.

Bourgouin, P.: A Method to Determine Precipitation Types, Weather and Forecasting, 15, 583–592, https://doi.org/10.1175/1520-0434(2000)015<0583:AMTDPT>2.0.CO;2, 2000.

Brun, E., David, P., Sudul, M., and Brunot, G.: A numerical model to simulate snow-cover stratigraphy for operational avalanche forecasting, Journal of Glaciology, 38, 13–22, https://doi.org/10.3189/S0022143000009552, 1992.

Cast, Z. I., Serreze, M. C., Cassano, E. N., and Barrett, A. P.: Seasonal characteristics and trends in precipitation partitioning in the Arctic, The Cryosphere, 20, 2127–2141, https://doi.org/10.5194/tc-20-2127-2026, 2026.

COSEWIC: COSEWIC assessment and status report on the Peary Caribou Rangifer tarandus pearyi in Canada, Tech. rep., Committee on the Status of Endangered Wildlife in Canada, Ottawa, http://www.registrelep-sararegistry.gc.ca/default_e.cfm, 2015.

Davison, T., Williams, J., and Adamczewski, J.: Aerial Survey of Peary Caribou (Rangifer tarandus pearyi) and Muskoxen (Ovibos moschatus) on Banks Island, July 2014, Manuscript Report 270, Environment and Natural Resources, Government of the Northwest Territories, https://www.gov.nt.ca/sites/ecc/files/resources/aerial_survey_of_peary_caribou_and_muskoxen_on_banks_island_-_july_2014.pdf, 2017.

Dolant, C., Langlois, A., Montpetit, B., Brucker, L., Roy, A., and Royer, A.: Development of a rain-on-snow detection algorithm using passive microwave radiometry, Hydrological Processes, 30, 3184–3196, https://doi.org/10.1002/hyp.10828, _eprint: https://onlinelibrary.wiley.com/doi/pdf/10.1002/hyp.10828, 2016.

Dolant, C., Langlois, A., Brucker, L., Royer, A., Roy, A., and Montpetit, B.: Meteorological inventory of rain-on-snow events and detection assessment in the Canadian arctic archipelago using passive microwave radiometry, in: 2017 IEEE International Geoscience and Remote Sensing Symposium (IGARSS), pp. 315–318, https://doi.org/10.1109/IGARSS.2017.8126959, iSSN: 2153-7003, 2017.

Dolant, C., Langlois, A., Brucker, L., Royer, A., Roy, A., and Montpetit, B.: Meteorological inventory of rain-on-snow events in the Canadian Arctic Archipelago and satellite detection assessment using passive microwave data, Physical Geography, 39, 428–444, https://doi.org/10.1080/02723646.2017.1400339, 2018.

https://doi.org/10.5194/egusphere-2026-6730
Preprint. Discussion started: 5 November 2026
© Author(s) 2026. CC BY 4.0 License.

Domine, F., Picard, G., Morin, S., Barrere, M., Madore, J.-B., and Langlois, A.: Major Issues in Simulating Some Arctic Snowpack Properties Using Current Detailed Snow Physics Models: Consequences for the Thermal Regime and Water Budget of Permafrost, Journal of Advances in Modeling Earth Systems, 11, 34–44, https://doi.org/10.1029/2018MS001445, _eprint: https://agupubs.onlinelibrary.wiley.com/doi/pdf/10.1029/2018MS001445, 2019.

Environment and Climate Change Canada: Glossary, https://climate.weather.gc.ca/glossary_e.html, entry: Precipitation.

Fierz, C., Armstrong, R., Durand, Y., Etchevers, P., Greene, E., McClung, D., Nishimura, K., Satyawali, P., and Sokratov, S.: The International Classification for Seasonal Snow on the Ground, IHP-VII Technical Documents in Hydrology 83, UNESCO-IHP, Paris, https://cryosphericsciences.org/wp-content/uploads/2019/02/snowclass_2009-11-23-tagged-highres.pdf, 2009.

Forbes, B. C., Kumpula, T., Meschtyb, N., Laptander, R., Macias-Fauria, M., Zetterberg, P., Verdonen, M., Skarin, A., Kim, K.-Y., Boisvert, L. N., Stroeve, J. C., and Bartsch, A.: Sea ice, rain-on-snow and tundra reindeer nomadism in Arctic Russia, Biology Letters, 12, https://doi.org/10.1098/rsbl.2016.0466, 2016.

French, H. M.: The Banks Island Tundra, in: Landscapes and Lanforms of Western Canada, World Geomorphological Landscapes, pp. 97–108, Springer, Cham, https://doi.org/https://doi.org/10.1007/978-3-319-44595-3_6, 2017.

Governement of Canada: Species at Risk Act (SARA), https://laws.justice.gc.ca/eng/acts/S-15.3/, last Modified: 2026-02-26, 2002.

Graham, R. M., Hudson, S. R., and Maturilli, M.: Improved Performance of ERA5 in Arctic Gateway Relative to Four Global Atmospheric Reanalyses, Geophysical Research Letters, 46, 6138–6147, https://doi.org/10.1029/2019GL082781, _eprint: https://agupubs.onlinelibrary.wiley.com/doi/pdf/10.1029/2019GL082781, 2019.

Grenfell, T. C. and Putkonen, J.: A method for the detection of the severe rain-on-snow event on Banks Island, October 2003, using passive microwave remote sensing, Water Resources Research, 44, https://doi.org/10.1029/2007WR005929, _eprint: https://onlinelibrary.wiley.com/doi/pdf/10.1029/2007WR005929, 2008.

Hansen, B., Isaksen, K., Benestad, R., Kohler, J., Pedersen, A., Loe, L., Coulson, S., Larsen, J., and Varpe, O.: Warmer and wetter winters: characteristics and implications of an extreme weather event in the High Arctic, Environmental Research Letters, 9, null, https://doi.org/10.1088/1748-9326/9/11/114021, 2014.

Hansen, B. B., Aanes, R., Herfindal, I., Kohler, J., and Sæther, B.-E.: Climate, icing, and wild arctic reindeer: past relationships and future prospects, Ecology, 92, 1917–1923, https://doi.org/10.1890/11-0095.1, 2011.

Harder, P. and Pomeroy, J.: Estimating precipitation phase using a psychrometric energy balance method, Hydrological Processes, 27, 1901–1914, https://doi.org/10.1002/hyp.9799, _eprint: https://onlinelibrary.wiley.com/doi/pdf/10.1002/hyp.9799, 2013.

Hersbach, H., Bell, B., Berrisford, P., Hirahara, S., Horányi, A., Muñoz-Sabater, J., Nicolas, J., Peubey, C., Radu, R., Schepers, D., Simmons, A., Soci, C., Abdalla, S., Abellan, X., Balsamo, G., Bechtold, P., Biavati, G., Bidlot, J., Bonavita, M., De Chiara, G., Dahlgren, P., Dee, D., Diamantakis, M., Dragani, R., Flemming, J., Forbes, R., Fuentes, M., Geer, A., Haimberger, L., Healy, S., Hogan, R. J., Hólm, E., Janisková, M., Keeley, S., Laloyaux, P., Lopez, P., Lupu, C., Radnoti, G., de Rosnay, P., Rozum, I., Vamborg, F., Villaume, S., and Thépaut, J.-N.: The ERA5 global reanalysis, Quarterly Journal of the Royal Meteorological Society, 146, 1999–2049, https://doi.org/10.1002/qj.3803, _eprint: https://onlinelibrary.wiley.com/doi/pdf/10.1002/qj.3803, 2020.

Jennings, K. S., Winchell, T. S., Livneh, B., and Molotch, N. P.: Spatial variation of the rain–snow temperature threshold across the Northern Hemisphere, Nature Communications, 9, 1148, https://doi.org/10.1038/s41467-018-03629-7, 2018.

Johnson, C. A., Neave, E., Blukacz-Richards, A., Banks, S., and Quesnelle, P.: Knowledge assessment (community and scientific) to inform the identification of critical habitat for Peary caribou, Rangifer tarandus pearyi, in the Canadian Arctic., Tech. rep., Environment and

https://doi.org/10.5194/egusphere-2026-6730
Preprint. Discussion started: 5 November 2026
© Author(s) 2026. CC BY 4.0 License.

Climate Change Canada, Science and Technology, Ottawa, Ontario, Canada, https://publications.gc.ca/collections/collection_2017/eccc/CW66-560-2017-eng.pdf, 2016.

Khedhaouiria, D., Gasset, N., Fortin, V., Dimitrijevic, M., Bulat, M., and Wang, X.: The Canadian Surface Reanalysis (CaSR) v3.2 precipitation dataset: A 45-year high-resolution analysis for North America (1980–2024), https://doi.org/10.5194/egusphere-2026-620, 2026.

Komarov, A. and Stroeve, J.: Local Controls on the Development of Percolation Features After a Rain-on-Snow Event in a Southern Taiga Snowpack, https://doi.org/10.5194/egusphere-2026-3873, 2026.

Kumpula, J., Parikka, P., and Nieminen, M.: Occurrence of certain microfungi on reindeer pastures in northern Finland during winter 1996-97, Rangifer, 20, 3–8, https://doi.org/10.7557/2.20.1.1477, 2000.

Lackner, G., Domine, F., Nadeau, D. F., Parent, A.-C., Anctil, F., Lafaysse, M., and Dumont, M.: On the energy budget of a low-Arctic snowpack, The Cryosphere, 16, 127–142, https://doi.org/10.5194/tc-16-127-2022, 2022.

Lafaysse, M., Cluzet, B., Dumont, M., Lejeune, Y., Vionnet, V., and Morin, S.: A multiphysical ensemble system of numerical snow modelling, The Cryosphere, 11, 1173–1198, https://doi.org/10.5194/tc-11-1173-2017, 2017.

Lafaysse, M., Dumont, M., De Fleurian, B., Fructus, M., Nheili, R., Viallon-Galinier, L., Baron, M., Boone, A., Bouchet, A., Brondex, J., Carmagnola, C., Cluzet, B., Fourteau, K., Haddjeri, A., Hagenmuller, P., Mazzotti, G., Minvielle, M., Morin, S., Quéno, L., Roussel, L., Spandre, P., Tuzet, F., and Vionnet, V.: Version 3.0.2 of the Crocus snowpack model, Geoscientific Model Development, 19, 6273–6334, https://doi.org/10.5194/gmd-19-6273-2026, 2026.

Langlois, A., Johnson, C., Montpetit, B., Royer, A., Blukacz-Richards, E. A., Neave, E., Dolant, C., Roy, A., Arhonditsis, G., Kim, D., Kaluskar, S., and Brucker, L.: Detection of rain-on-snow (ROS) events and ice layer formation using passive microwave radiometry: A context for Peary caribou habitat in the Canadian Arctic, Remote Sensing of Environment, 189, 84–95, https://doi.org/10.1016/J.RSE.2016.11.006, 2017.

Langlois, J.-A., Langlois, A., Dolant, C., Johnson, C. A., and Sachs Harbour Hunters & Trappers Committee, R. B. H. . T. A.: Drivers, detection and impacts of rain-on-snow events on Banks Island, Canadian Arctic Archipelago: insights from remote sensing and Inuit Knowledge, Polar Research, 45, https://doi.org/10.33265/polar.v45.12930, 2026.

Laptander, R., Horstkotte, T., Habeck, J. O., Rasmus, S., Komu, T., Matthes, H., Tømmervik, H., Istomin, K., Eronen, J. T., and Forbes, B. C.: Critical seasonal conditions in the reindeer-herding year: A synopsis of factors and events in Fennoscandia and northwestern Russia, Polar Science, 39, 101 016, https://doi.org/10.1016/j.polar.2023.101016, 2024.

Laroche, S. and Poan, E. D.: Impact of the Arctic observing systems on the ECCC global weather forecasts, Quarterly Journal of the Royal Meteorological Society, 148, 252–271, https://doi.org/10.1002/qj.4203, _eprint: https://rmets.onlinelibrary.wiley.com/doi/pdf/10.1002/qj.4203, 2022.

Larter, N. and Nagy, J.: Ice conditions survey, Banks Island October/November 1993, Tech. Rep. Manuscript Report No. 77, Department of Renewable Resources, Government of the Northwest Territories, Inuvik, NWT, 1994.

Lauer, M., Rinke, A., Gorodetskaya, I., Sprenger, M., Mech, M., and Crewell, S.: Influence of atmospheric rivers and associated weather systems on precipitation in the Arctic, Atmospheric Chemistry and Physics, 23, 8705–8726, https://doi.org/10.5194/acp-23-8705-2023, 2023.

Lawrence, H., Bormann, N., Sandu, I., Day, J., Farnan, J., and Bauer, P.: Use and impact of Arctic observations in the ECMWF Numerical Weather Prediction system, Quarterly Journal of the Royal Meteorological Society, 145, 3432–3454, https://doi.org/10.1002/qj.3628, _eprint: https://rmets.onlinelibrary.wiley.com/doi/pdf/10.1002/qj.3628, 2019.

https://doi.org/10.5194/egusphere-2026-6730
Preprint. Discussion started: 5 November 2026
© Author(s) 2026. CC BY 4.0 License.

Leroux, N. R., Vionnet, V., and Thériault, J. M.: Performance of precipitation phase partitioning methods and their impact on snowpack evolution in a humid continental climate, Hydrological Processes, 37, e15 028, https://doi.org/10.1002/hyp.15028, _eprint: https://onlinelibrary.wiley.com/doi/pdf/10.1002/hyp.15028, 2023.

Li, L. and Pomeroy, J. W.: Estimates of Threshold Wind Speeds for Snow Transport Using Meteorological Data, Journal of Applied Meteorology and Climatology, 36, 205–2013, https://doi.org/10.1175/1520-0450(1997)036<0205:EOTWSF>2.0.CO;2, 1997.

Liston, G. E. and Elder, K.: A Distributed Snow-Evolution Modeling System (SnowModel), Journal of Hydrometeorology, 7, 1259–1276, https://doi.org/10.1175/JHM548.1, 2006.

Loeb, N. A., Crawford, A., Stroeve, J. C., and Hanesiak, J.: Frontiers | Extreme Precipitation in the Eastern Canadian Arctic and Greenland: An Evaluation of Atmospheric Reanalyses, Frontiers in Environmental Science, 10, https://doi.org/10.3389/fenvs.2022.866929, 2022.

Madore, J.-B., Langlois, A., and Fierz, C.: Temporal Analysis of Snow Stratigraphy and Melt–Freeze Crusts Using a 24 Ghz Frequency Modulated Continuous Wave (Fmcw) Radar in Avalanche Terrain, https://doi.org/10.2139/ssrn.4530309, 2023.

Markkula, I., Turunen, M., Rasmus, S., Rikkonen, T., Koski, V., and Welker, J. M.: Changing Winter Landscapes: Extreme Weather Events and Meanings of Snow for Sámi Reindeer Herders, ARCTIC, 77, 197–216, https://doi.org/10.14430/arctic80385, 2025.

Marsh, P. and Pomeroy, J. W.: Meltwater fluxes at an Arctic forest-tundra site, Hydrological Processes, 10, 1383–1400, https://doi.org/10.1002/(SICI)1099-1085(199610)10:10<1383::AID-HYP468>3.0.CO;2-W, 1996.

Martineau, C., Langlois, A., Gouttevin, I., Neave, E., and Johnson, C. A.: Improving Peary Caribou Presence Predictions in MaxEnt Using Spatialized Snow Simulations, Arctic, 75, 55–71, https://www.jstor.org/stable/27211974, 2022.

McCrystall, M. R., Stroeve, J., Serreze, M., Forbes, B. C., and Screen, J. A.: New climate models reveal faster and larger increases in Arctic precipitation than previously projected, Nature Communications, 12, 6765, https://doi.org/10.1038/s41467-021-27031-y, 2021.

Menard, C. B., Rasmus, S., Merkouriadi, I., Balsamo, G., Bartsch, A., Derksen, C., Domine, F., Dumont, M., Ehrich, D., Essery, R., Forbes, B. C., Krinner, G., Lawrence, D., Liston, G., Matthes, H., Rutter, N., Sandells, M., Schneebeli, M., and Stark, S.: Exploring the decision-making process in model development: focus on the Arctic snowpack, The Cryosphere, 18, 4671–4686, https://doi.org/10.5194/tc-18-4671-2024, 2024.

Miller, F. L. and Gunn, A.: Catastrophic Die-off of Peary Caribou on the Western Queen Elizabeth Islands, Canadian High Arctic, Arctic, 56, 381–390, https://www.jstor.org/stable/40513077, 2003.

Mudryk, L., Santolaria-Otín, M., Krinner, G., Ménégoz, M., Derksen, C., Brutel-Vuilmet, C., Brady, M., and Essery, R.: Historical Northern Hemisphere snow cover trends and projected changes in the CMIP6 multi-model ensemble, The Cryosphere, pp. 2495–2514, https://doi.org/10.5194/tc-14-2495-2020, 2020.

Nagy, J. A., Larter, N. C., and Fraser, V. P.: Population demography of Peary caribou and muskox on Banks Island, N.W.T., 1982-1992, Rangifer, pp. 213–222, https://doi.org/10.7557/2.16.4.1245, 1996.

Obarein, O. A. and Lee, C. C.: ERA5 Reproduces Key Features of Global Precipitation Trends in A Warming Climate, International Journal of Climatology, 45, e8877, https://doi.org/10.1002/joc.8877, 2025.

Oleson, K., YJ, D., GB, B., Bosilovich, M., Dickinson, R., Dirmeyer, P., Hoffman, F., Houser, P., Levis, S., Niu, G.-Y., Thornton, P., Vertenstein, M., Yang, Z.-L., and XB, Z.: Technical Description of the Community Land Model (CLM), NCAR Technical Note NCAR/TN-461+STR, National Center for Atmospheric Research, Boulder, CO, https://doi.org/10.5065/D6N877R0, nCAR/TN-461+STR, 2004.

Ouellet, F., Langlois, A., Blukacz-Richards, E. A., Johnson, C. A., Royer, A., Neave, E., and Larter, N. C.: Spatialization of the SNOWPACK snow model for the Canadian Arctic to assess Peary caribou winter grazing conditions, Physical Geography, 38, 143–158, https://doi.org/10.1080/02723646.2016.1274200, 2017.

https://doi.org/10.5194/egusphere-2026-6730
Preprint. Discussion started: 5 November 2026
© Author(s) 2026. CC BY 4.0 License.

Overland, J. E.: Rare events in the Arctic, Climatic Change, 168, 27, https://doi.org/10.1007/s10584-021-03238-2, 2021.

Pan, C. G., Kirchner, P. B., Kimball, J. S., Kim, Y., and Du, J.: Rain-on-snow events in Alaska, their frequency and distribution from satellite observations, Environmental Research Letters, 13, 075 004, https://doi.org/10.1088/1748-9326/aac9d3, 2018.

Parks Canada Agency, G. o. C.: Aulavik National Park, https://parks.canada.ca/pn-np/nt/aulavik, last Modified: 2026-07-13, 2025.

Pernov, J. B., Gros-Daillon, J., and Schmale, J.: Comparison of selected surface level ERA5 variables against in-situ observations in the continental Arctic, Quarterly Journal of the Royal Meteorological Society, 150, 2123–2146, https://doi.org/10.1002/qj.4700, _eprint: https://rmets.onlinelibrary.wiley.com/doi/pdf/10.1002/qj.4700, 2024.

Pflug, J. M., Liston, G. E., Nijssen, B., and Lundquist, J. D.: Testing Model Representations of Snowpack Liquid Water Percolation Across Multiple Climates, Water Resources Research, 55, 4820–4838, https://doi.org/10.1029/2018WR024632, _eprint: https://agupubs.onlinelibrary.wiley.com/doi/pdf/10.1029/2018WR024632, 2019.

Poggio, L., de Sousa, L. M., Batjes, N. H., Heuvelink, G. B. M., Kempen, B., Ribeiro, E., and Rossiter, D.: SoilGrids 2.0: producing soil information for the globe with quantified spatial uncertainty, Soil, 7, 217–240, https://doi.org/10.5194/soil-7-217-2021, 2021.

Putkonen, J., Grenfell, T. C., Rennert, K., Bitz, C., Jacobson, P., and Russell, D.: Rain on Snow: Little Understood Killer in the North, Eos, Transactions American Geophysical Union, 90, 221–222, https://doi.org/10.1029/2009EO260002, _eprint: https://agupubs.onlinelibrary.wiley.com/doi/pdf/10.1029/2009EO260002, 2009.

Quéno, L., Vionnet, V., Cabot, F., Vrécourt, D., and Dombrowski-Etchevers, I.: Forecasting and modelling ice layer formation on the snowpack due to freezing precipitation in the Pyrenees, Cold Regions Science and Technology, 146, 19–31, https://doi.org/10.1016/j.coldregions.2017.11.007, 2018.

Rasmus, S., Kivinen, S., and Irannezhad, M.: Basal ice formation in snow cover in Northern Finland between 1948 and 2016, Environmental Research Letters, 13, 114 009, https://doi.org/10.1088/1748-9326/aae541, 2018.

Rasmus, S., Turunen, M., Luomaranta, A., Kivinen, S., Jylhä, K., and Räihä, J.: Climate change and reindeer management in Finland: Co-analysis of practitioner knowledge and meteorological data for better adaptation, Science of The Total Environment, 710, 136 229, https://doi.org/10.1016/j.scitotenv.2019.136229, 2020.

Rennert, K., Roe, G., Putkonen, J., and Bitz, C.: Soil thermal and ecological impacts of rain on snow events in the circumpolar arctic, Journal of Climate, 22, 2302–2315, https://doi.org/10.1175/2008JCLI2117.1, 2009.

Riseth, J. A., Tommervik, H., Helander-Renvall, E., Labba, N., Johansson, C., Malnes, E., Bjerke, J. W., Jonsson, C., Pohjola, V., Sarri, L.-E., Schanche, A., and Callaghan, T. V.: Sámi traditional ecological knowledge as a guide to science: snow, ice and reindeer pasture facing climate change, Polar Record, 47, 202–217, https://doi.org/10.1017/S0032247410000434, 2011.

Robinson, D. A., Estilow, T. W., and Program, N. C.: NOAA Climate Data Record (CDR) of Northern Hemisphere (NH) Snow Cover Extent (SCE), Version 1, NOAA National Centers for Environmental Information, https://doi.org/10.7289/V5N014G9, last Modified: 2026-06-11, 2012.

Royer, A., Domine, F., Roy, A., Langlois, A., Marchand, N., and Davesne, G.: New northern snowpack classification linked to vegetation cover on a latitudinal mega-transect across northeastern Canada, Écoscience, 28, 225–242, https://doi.org/10.1080/11956860.2021.1898775, 2021a.

Royer, A., Picard, G., Vargel, C., Langlois, A., Gouttevin, I., and Dumont, M.: Improved Simulation of Arctic Circumpolar Land Area Snow Properties and Soil Temperatures, Frontiers in Earth Science, https://doi.org/10.3389/feart.2021.685140, 2021b.

https://doi.org/10.5194/egusphere-2026-6730
Preprint. Discussion started: 5 November 2026
© Author(s) 2026. CC BY 4.0 License.

Sasseville, V., Langlois, A., Brucker, L., and Johnson, C. A.: Patterns and Trend Analysis of Rain-on-Snow Events using Passive Microwave Satellite Data over the Canadian Arctic Archipelago Since 1987, Journal of Hydrometeorology, 25, 311–324, https://doi.org/10.1175/JHM-D-22-0218.1, aDS Bibcode: 2024JHyMe..25..311S, 2024.

Schleef, S., Löwe, H., and Schneebeli, M.: Influence of stress, temperature and crystal morphology on isothermal densification and specific surface area decrease of new snow, The Cryosphere, 8, 1825–1838, https://doi.org/10.5194/tc-8-1825-2014, 2014.

Serreze, M. C., Gustafson, J., Barrett, A. P., Druckenmiller, M. L., Fox, S., Voveris, J., Stroeve, J., Sheffield, B., Forbes, B. C., Rasmus, S., Laptander, R., Brook, M., Brubaker, M., Temte, J., McCrystall, M. R., and Bartsch, A.: Arctic rain on snow events: bridging observations to understand environmental and livelihood impacts, Environmental Research Letters, 16, 105 009, https://doi.org/10.1088/1748-9326/ac269b, 2021.

Serreze, M. C., Voveris, J., Barrett, A. P., Fox, S., Blanken, P. D., and Crawford, A.: Characteristics of extreme daily precipitation events over the Canadian Arctic, International Journal of Climatology, 42, 10 353–10 372, https://doi.org/10.1002/joc.7907, _eprint: https://onlinelibrary.wiley.com/doi/pdf/10.1002/joc.7907, 2022.

Stien, A., Loe, L. E., Mysterud, A., Severinsen, T., Kohler, J., and Langvatn, R.: Icing events trigger range displacement in a high-arctic ungulate, Ecology, 91, 915–920, https://doi.org/10.1890/09-0056.1, 2010.

Taylor, A. D. M.: Inuit Qaujimajatuqangit about Population Changes and Ecology of Peary Caribou and Muskoxen on the High Arctic Islands of Nunavut, Ph.D. thesis, Queen's University, Kingston, Ontario, Canada, 2005.

Teufelsbauer, H.: A two-dimensional snow creep model for alpine terrain, Natural Hazards, 56, 481–497, https://doi.org/10.1007/s11069-010-9515-8, 2011.

Tomaselli, M., Gerlach, S. C., Kutz, S. J., Checkley, S. L., and Iqaluktutiaq, C. o.: Iqaluktutiaq Voices: Local Perspectives about the Importance of Muskoxen, Contemporary and Traditional Use and Practices, Arctic, 71, 1–14, https://www.jstor.org/stable/26387326, 2018.

Vickers, H., Malnes, E., and Eckerstorfer, M.: A Synthetic Aperture Radar Based Method for Long Term Monitoring of Seasonal Snowmelt and Wintertime Rain-On-Snow Events in Svalbard, Frontiers in Earth Science, 10, https://doi.org/10.3389/feart.2022.868945, 2022.

Vikhamar-Schuler, D., Hanssen-Bauer, I., Schuler, T. V., Mathiesen, S. D., and Lehning, M.: Use of a multilayer snow model to assess grazing conditions for reindeer, Annals of Glaciology, 54, 214–226, https://doi.org/10.3189/2013AoG62A306, 2013.

Vionnet, V., Brun, E., Morin, S., Boone, A., Faroux, S., Le Moigne, P., Martin, E., and Willemet, J.-M.: The detailed snowpack scheme Crocus and its implementation in SURFEX v7.2, Geoscientific Model Development, 5, 773–791, https://doi.org/10.5194/gmd-5-773-2012, 2012.

Vionnet, V., Leroux, N. R., Fortin, V., Abrahamowicz, M., Woolley, G., Mazzotti, G., Gaillard, M., Lafaysse, M., Royer, A., Domine, F., Gauthier, N., Rutter, N., Derksen, C., and Bélair, S.: Enhancing simulations of snowpack properties in land surface models with the Soil, Vegetation and Snow scheme v2.0 (SVS2), Geoscientific Model Development, 18, 9119–9147, https://doi.org/10.5194/gmd-18-9119-2025, 2025.

Voveris, J. J.: Meteorological Drivers of Arctic Rain-On-Snow Events and How Climate Change May Influence Associated Risks, Master's thesis, University of Colorado, Boulder, CO, https://www.proquest.com/docview/2681751208, proQuest document ID: 2681751208 and ProQuest publication number: 29069573, 2022.

Wang, X. L., Xu, H., Qian, B., Feng, Y., and Mekis, E.: Adjusted Daily Rainfall and Snowfall Data for Canada, Atmosphere-Ocean, 55, 155–168, https://doi.org/10.1080/07055900.2017.1342163, 2017.

Wang, Y.-H., Broxton, P., Fang, Y., Behrangi, A., Barlage, M., Zeng, X., and Niu, G.-Y.: A Wet-Bulb Temperature-Based Rain-Snow Partitioning Scheme Improves Snowpack Prediction Over the Drier Western United States, Geophysical Research Letters, 46, 13 825–13 835, https://doi.org/10.1029/2019GL085722, _eprint: https://agupubs.onlinelibrary.wiley.com/doi/pdf/10.1029/2019GL085722, 2019.

https://doi.org/10.5194/egusphere-2026-6730
Preprint. Discussion started: 5 November 2026
© Author(s) 2026. CC BY 4.0 License.



Wever, N., Fierz, C., Mitterer, C., Hirashima, H., and Lehning, M.: Solving Richards Equation for snow improves snowpack meltwater runoff estimations in detailed multi-layer snowpack model, The Cryosphere, 8, 257–274, https://doi.org/10.5194/tc-8-257-2014, 2014.

Woo, M.-k. and Heron, R.: Occurrence of Ice Layers at the Base of High Arctic Snowpacks, Arctic and Alpine Research, 13, 225–230, https://doi.org/10.1080/00040851.1981.12004242, 1981.

Woolley, G. J., Rutter, N., Wake, L., Vionnet, V., Derksen, C., Essery, R., Marsh, P., Tutton, R., Walker, B., Lafaysse, M., and Pritchard, D.: Multi-physics ensemble modelling of Arctic tundra snowpack properties, The Cryosphere, 18, 5685–5711, https://doi.org/10.5194/tc-18-5685-2024, 2024.

Würzer, S., Jonas, T., Wever, N., and Lehning, M.: Influence of Initial Snowpack Properties on Runoff Formation during Rain-on-Snow Events, Journal of Hydrometeorology, 17, 1801–1815, https://doi.org/10.1175/JHM-D-15-0181.1, 2016.